이학박사 학위논문

I. **Efficient dermal delivery of retinyl palmitate: Progressive polarimetry and Raman spectroscopy to evaluate the structure and efficacy**

II. **Liquid crystal nanoparticle formulation as an oral drug delivery system for liver-specific distribution**

I. 편광측정법과 라만분광법을 이용한 액정에멀전의 구조 분석 및 레티닐 팔미테이트의 피부전달 영향 연구

II. 간에 선택적인 경구투여 약물전달 체계로서 액정나노입자 제형 연구

2016년 8월

서울대학교 대학원

화학부 유기화학 전공

이 동 렬

CONTENTS

Abstract

Part I. Efficient dermal delivery of retinyl palmitate: Progressive polarimetry and Raman spectroscopy to evaluate the structure and efficacy*

Over the past decades, there has been a growing interest in dermal drug delivery. Although various novel delivery devices and methods have been developed, dermal delivery is still challenging because of problems such as poor drug permeation, instability of vesicles and drug leakage from vesicles induced by fusion of vesicles. To solve the vesicle instability problems in current dermal delivery systems, we developed materials comprised of liquid crystals as a new delivery vehicle of retinyl palmitate and report the characterization of the liquid crystals using a Mueller matrix polarimetry. The stability of the liquid-crystal materials was evaluated using the polarimeter as a novel evaluation tool along with other conventional methods. The dermal delivery of retinyl palmitate was investigated through the use of confocal Raman spectroscopy. The results indicate that the permeation of retinyl palmitate was enhanced by up to 106% compared to that using an ordinary emulsion with retinyl palmitate.

Key words: Liquid-crystal emulsion, retinyl palmitate, dermal delivery, Mueller matrix polarimeter, confocal Raman spectroscopy

*Part of this thesis was published in *Eur. J. Pharm. Sci.* **2015**, *78*, 111–120.

Part II. Liquid crystal nanoparticle formulation as an oral drug delivery system for liver-specific distribution[†]

Liquid crystal nanoparticles have been utilized as an efficient tool for drug delivery with enhanced bioavailability, drug stability, and targeted drug delivery. However, the high energy requirements and the high cost of the liquid crystal preparation have been obstacles to their widespread use in the pharmaceutical industry. In this study, we prepared liquid crystal nanoparticles using a phase-inversion temperature method, which is a uniquely low energy process. Particles prepared with above method were estimated to be around 100 nm in size and exhibited a lamellar liquid crystal structure with orthorhombic lateral packing. Pharmacokinetic and tissue distribution studies of a hydrophobic peptide-based drug candidate formulated with the liquid crystal nanoparticles showed a five-fold enhancement of bioavailability, sustained release, and liver-specific drug delivery compared to a host–guest complex formulation.

Keywords: LCNP, PIT, Sustained release, Bioavailability, Liver-specific

[†]Part of this thesis was published in *Int. J. Nanomed.* **2016**, *11*, 853-871.

List of Figures

Part I.

Figure 9. Spectrum of the LC emulsion without RP (a) and with RP (b) in confocal Raman spectroscopy. The different peaks of the emulsion with RP are 1162, 1194 and 1596 cm^{-1}.

Figure 10. Dermal delivery of RP incorporated into the LC emulsion (a) and the ordinary emulsion (b) in the randomized in vivo trial.

Part II.

Figure 1. Ternary phase diagram of the surfactant complex, tetradecyl tetradecanoate, and water. The dotted triangle indicates the compositions at which the liquid crystal nanoparticles (LCNPs) can be prepared. The composition of LCNP-#8 is designated by a dark dot (•).

Figure 2. Conductivity of liquid crystal nanoparticles (LCNP)-#8 on heating. A semi-transparent phase appeared as the conductivity decreased from 80℃.

Figure 3. HPLC analysis of BMK-20113 incorporated into the liquid crystal nanoparticle (LCNP); (a) BMK-20113 in tetrahydrofuran, (b) LCNP-#8 and (c) LCNP-#11.

Figure 4. Evaluation of the physicochemical properties of the liquid crystal nanoparticles (LCNPs); (a) small angle x-ray diffraction (SAXD) and (b) wide angle x-ray diffraction (WAXD) of LCNP-#8, #9, #10, and #11. The lamellar liquid crystal structure is indicated by the sequential peaks positioned at 0.65 and 1.3 (nm^{-1}) in the SAXD. In the WAXD, the peaks positioned at 15.0 and 16.6 (nm^{-1}) correspond to the

orthorhombic lateral packing structure. No significant changes were observed with varying concentrations of BMK-20113.

Figure 5. Illustration of the structure of the prepared liquid crystal nanoparticles (LCNPs). The interphase of the LCNPs is comprised of a lamellar liquid crystal structure with orthorhombic lateral packing.

Figure 6. The differential scanning calorimetry (DSC) curves for liquid crystal nanoparticles (LCNP)-#8, #9, #10, and #11. The main peaks from 33 to 36℃ and the small peaks at 25 and 32℃ for LCNP-#8 did not change significantly with increasing concentrations of BMK-20113.

Figure 7. The differential scanning calorimetry (DSC) results of Emulgade SE-PF (a), tetradecyl tetradecanoate (b) and PEG-12 cetostearyl ether (c)

Figure 8. Transmission electron microscopy (TEM) images of liquid crystal nanoparticles (LCNP)-#8, #9, #10, and #11.

Figure 9. Transmission Electron Microscopy (TEM) image of BMK-20113 recrystallization of LCNP-#12

Figure 10. Transmission Electron Microscopy (TEM) image of LCNP-#8 and #11 in an acidic condition (pH 1.5

Figure 11. Stability of liquid crystal nanoparticles (LCNP)-#8, #9, #10, and #11 at (a) 4℃ and (b) 37℃. LCNP-#8 and #9 are stable at 4℃ and 37℃ for 2 months, while LCNP-#10 and #11 are stable at 4℃ for 2 months and at 37℃ for 1 week.

Figure 12. Cumulative release (0–72 h) of BMK-20113 from the host–guest complex (HGC, control solution) and liquid crystal nanoparticles (LCNP-#11); n = 3.

Figure 13. Plasma concentrations (nmol/L) of BMK-20113 incorporated in host–guest complex (HGC) and liquid crystal nanoparticles (LCNPs)-#11 in male Sprague-Dawley rats after a 10 mg/kg oral (PO) dose, n = 5.

Figure 14. Concentrations and tissue distributions of BMK-20113 incorporated into host–guest complex (HGC) and liquid crystal nanoparticles (LCNP)-#11. (a) Concentrations of BMK-20113 in tissues, in male Sprague-Dawley rats 5 min after a 5 mg/kg intravenous (IV) dose of BMK-20113 incorporated into HGC or LCNP-#11, n = 3. (b) Ratio of the concentration of BMK-20113 in tissue to that in plasma after oral dose of BMK-20113 incorporated into HGC or LCNP-#11. CSF, cerebrospinal fluid.

List of Tables

Part I.

Part II.

Part I.

Efficient Dermal Delivery of Retinyl Palmitate: Progressive Polarimetry and Raman Spectroscopy to Evaluate the Structure and Efficacy

I. Introduction

Dermal drug delivery has been intensively studied in pharmaceutical and dermatological applications because the chemical and enzymatic degradation of active ingredients in the gastrointestinal tract and liver in oral administration can be avoided and the controlled release of a drug can be achieved.[1] However, permeation through the main barrier of the skin, stratum corneum (SC), can be difficult because it protects the organism from the permeation of drugs or other chemicals with a lipid-rich composition and its lamellar liquid-crystalline structure.[2] It has also been reported that the brick-and-mortar structure of the SC along with keratin corneocytes contributes to the poor permeation of water and oil-soluble chemicals with molecular weights >500 Da.[3] To overcome these limitations, attempts have been made to use chemical permeation enhancers, microemulsions, liposomes as encapsulated carriers, solid lipid nanoparticles, ethosomes, and liquid-crystal (LC) emulsions. However, skin irritation was reported as a potential adverse consequence of the permeation enhancers.[4] The microemulsions could also be associated with the destabilization and precipitation of drugs.[5] Permeation and safety could be improved using liposomes; however, there have been limitations in applications for the pharmaceutical industry because of chemical and physical stability issues with liposome aggregation and degradation of drug.[6] Solid lipid nanoparticles have been used to overcome the limitations of liposomes, because the drug leakage problem could be solved with the improved permeation, long term physical stability and slow degradation of drugs; however, harsh preparation conditions are still problematic.[7] Because of the enhanced permeability of ethosomes, they have also been studied as a novel dermal carrier; however, securing physical stability of ethosomes is still challenging.[8]

Since the advent of LC emulsions by Friberg composed of carboxylic acids, water, and oil, many studies have indicated that LC emulsions can be applied in topical applications as an SC permeation enhancer.[9] Because LC emulsions can be considered as a mimic of the SC, which is composed of an LC structure, biological performances such as the improvement of the skin barrier function and controlled drug release are possible.[9c, 10] Compared to conventional emulsions, hydrophilic and lipophilic chemicals incorporated in LC emulsions show improved SC permeability because the LC mesophase of chemicals may interact with the LC structure of human skin.[9d] Although LC emulsions are generally more stable than conventional ones due to the well-ordered arrangement of lipids,[11] the long-term instability of LC emulsions can be problematic, since the thermal motion of lipid and emulsifier molecules can gradually decompose the LC structure.[12]

Retinoids and their analogs have received much attention in skin aging therapy because these chemicals are multifunctionally related to the regulation of epithelial cell growth and collagen synthesis.[13] However, due to the safety concern regarding retinoids, their analogs have been used as alternatives, such as retinyl palmitate (RP) and retinyl acetate.[14] The dermal delivery of RP has received much attention because the delivery of RP could not be accomplished efficiently without an optimized delivery system due to the high molecular weight of RP.[15] Permeation has been improved using chemical permeation enhancers; however, they cause skin irritation.[4]

The evaluation of LC structures has been a key issue in the study of LC emulsions, and it has been achieved qualitatively by X-ray scattering, differential scanning calorimeter (DSC), and cryo-transmission electron microscopy (cryo-TEM).[16] X-ray scattering is appropriate for the identification of the periodicity of the LC structure by simple calculations using Bragg's equation.[17] Another measurement method, DSC, was used for evaluating the stability of LC emulsions; for example, the preservation of

enthalpy indicated that the LC structure would not be changed under experimental conditions.[9c] Cryo-TEM provides a direct observation of LC emulsion structures; however, highly experienced professionals are generally required for the analysis because the deformation of the LC structure can occur during the preprocessing of samples. Moreover, these test methods are not appropriate for the estimation of the degree of LC structure formation which is observed as beam polarization; therefore, the change in the physicochemical properties of the LC structure has been difficult to measure with traditional methods. The degree of polarization has been measured using a Mueller matrix polarimeter (MMP);[18] however, to the best of our knowledge, the application has been limited to size determination and observation of the phase behavior of LC display.[19]

In this study, we report the 1) characterization of the LC structure using MMP, and 2) enhanced dermal delivery of RP with LC emulsion. The LC emulsions were metastable with the optimized composition of fatty alcohols, emulsifiers, ceramides and other additives. The structures of the LC emulsions were characterized by conventional methods using polarized microscopy, small-angle X-ray diffraction (SAXD), wide-angle X-ray diffraction (WAXD), DSC, and cryo-scanning electron microscopy (cryo-SEM), and the results obtained were compared with those obtained using MMP. The degree and quantities of LC formation were evaluated with the retardance values of the polarized beam from MMP, and the values of the LC emulsions under stability test were compared to that of the standard sample to confirm the stability of the LC structure. To evaluate the efficacy of LC emulsions in the dermal delivery of RP, the confocal Raman spectroscopy was employed, which has been introduced as a noninvasive *in vivo* method providing skin molecular composition as a function of skin depth.[20] Furthermore, it was reported that the quantitative analysis of *trans*-retinol is possible by normalizing all spectra with the keratin signal.[21] From the studies, the

spectroscopy proved to be a convenient and powerful tool for the evaluation of the penetration of RP *in vivo* over multiple depth and time points without skin damage, which can be induced by conventional methods such as skin biopsy or tape stripping.[22]

II. Result and Discussion

Evaluation of liquid-crystalline phase behavior by DSC. The compositions of LC emulsions and ordinary emulsions are shown in Table 1. The ingredients of both emulsions are the same; except that PEG-100 stearate was applied in the ordinary emulsions while the alkyl glucoside and sorbitan palmitate were incorporated into LC emulsions, which function as promoters of LC structure formation. In Figure 1(a) the original peaks of 1-hexadecanol and 1-octadecanol correspond to each melting point, respectively. In case of the LC emulsion, only one single peak was detected at about 48 ℃ as shown in Figure 1(b) and the integration value of the peak of the LC emulsion is 11.8 J/g, which was much larger than that of the ordinary emulsion, 2.23 J/g (Fig 1(c)). From this observation, it can be postulated that the interaction of 1-hexadecanol and 1-octadecanol is strong enough to form the homogeneous phase with the phase transition at 48 ℃. Additionally, it was found that the Lα phase exists up to 60 °C for LC emulsion, as shown in Figure 1(b). The Lα phase changed to the Lβ phase below the transition temperature, Tc, and the fatty alcohols could migrate into the water phase because a smaller number of fatty alcohol molecules was required to form the Lβ phase than that of the Lα phase. When the LC emulsion was incorporated with C12–20 alkyl glucoside, sorbitan palmitate and hydrogenated lecithin, Tc was ~48 ℃, and the phase transition did not complete up to 60 ℃. Therefore, the dominant structure at 40 and 50 °C was Lα. From the elevation of Tc in LC emulsion, it can be concluded that C12-13 alkyl glucoside and sorbitan palmitate contribute to the delay of LC structure swelling, which results in the stabilization of LC structure better than PEG-100 stearate does because the ordinary emulsion and LC emulsion differ only in the type of surfactants

Table 1. Composition of the samples for MMP and confocal Raman spectroscopy.

	Ingredient[a]	Ordinary Emulsion	LC Emulsion
A	C12-20 alkyl glucoside	0	1.00
	Sorbitan palmitate	0	1.00
	PEG-100 stearate	2.00	0
	1-Hexadecanol	3.00	3.00
	1-Octadecanol	1.00	1.00
	Caprylic/capric triglyceride	5.00	5.00
	Retinyl Palmitate	0.60	0.60
B	Water	To 100	To 100
	Glycerin	5.00	5.00
	Dipropylene glycol	5.00	5.00

[a] Additives are glyceryl stearate (0.50%), ceramides-3 (0.25%), cholesterol (0.25%), stearic acid (0.50%) and hydrogenated lecithin (0.10%) in part A and disodium ethylenediaminetetraacetic acid (0.02%), triethyl-amine (adjust to pH 7.5) and carbomer (0.10%) in part B.

Figure 1. (a) DSC of 1-hexadecanol and 1-octadecanol; (b) DSC of LC emulsion; (c) DSC of ordinary emulsion

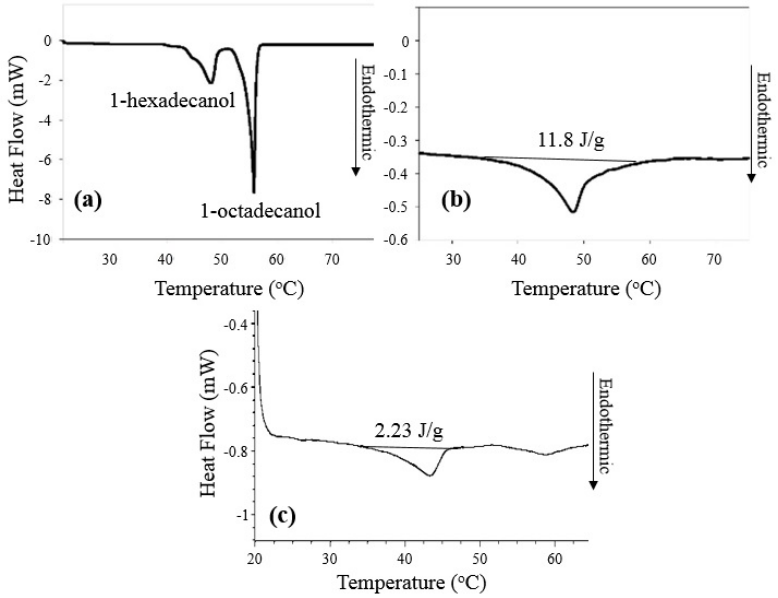

Structure assessment of prepared liquid-crystal emulsion by SAXD and WAXD. The structure of LC emulsion with RP was evaluated with the aid of SAXD and WAXD. In the WAXD pattern shown in Figure 2(a), an indexing peak appeared at 21.3°, which is consistent with the reported hexagonally packed structure of LC emulsions, as shown in Eq. 1.[23] The phase of hexagonal lateral packing parallel to the surface plane of emulsion droplet and the directions of hydrocarbon chains of emulsifiers and fatty alcohols are perpendicular to the phase. In the hexagonal lateral packing, the distances between the hydrocarbon chains are equal with 0.417 nm spacing.

Figure 2. (a) WAXD of LC emulsion (b) SAXD of LC emulsion

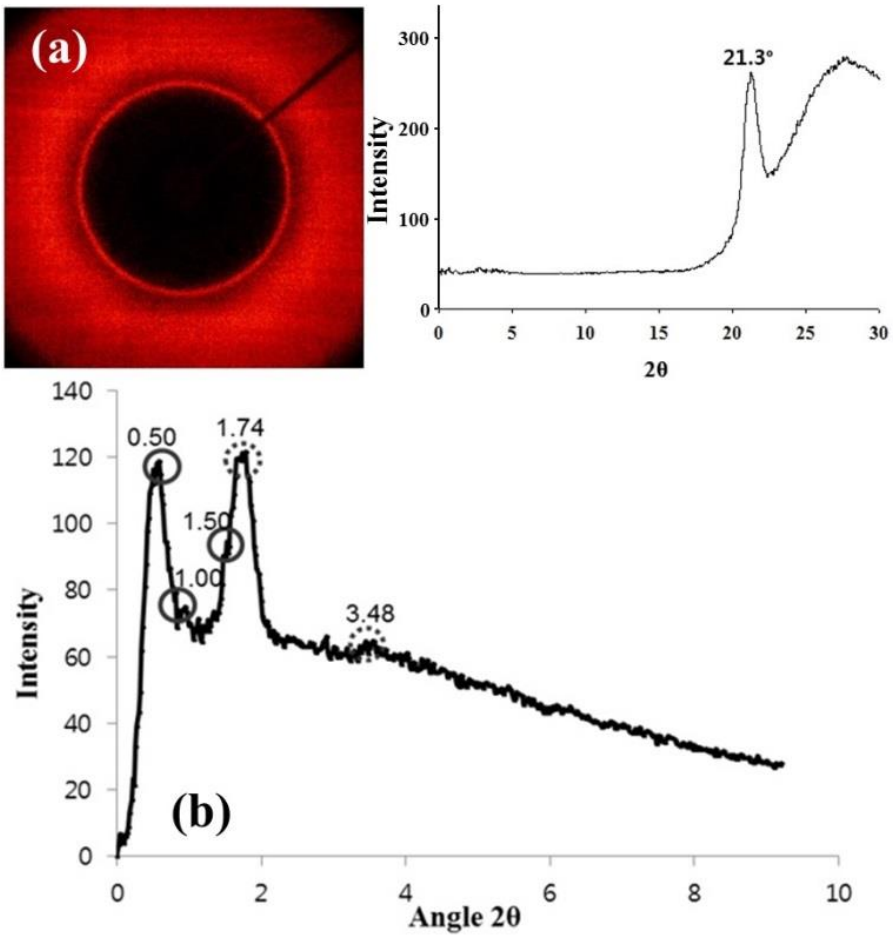

$$d = \lambda/2\sin\theta = 0.154 \text{ nm}/2\sin(21.3/2) = 0.417 \text{ nm} \quad \text{(Eq. 1.)}$$

In the SAXD pattern shown in Figure 2(b), two types of repeated phase are observed: One is a long periodicity phase (LPP) with the indexing peaks at 0.50°, 1.00°, and 1.50°, and another is a short periodicity phase (SPP) with the indexing peaks at 1.74° and 3.48°. The distance between the planes of LPP and SPP is 176.5 and 50.7 Å, respectively, which are similar to the reported values of LC in SC, 128 and 56 Å for LPP and SPP, respectively,. From these calculations, it can be concluded that the structure of LC emulsion is a multi-lamellar LC system with hexagonal packing, similar to that of SC, as it is described in Figure 3.[23]

Figure 3. Illustration of the LC emulsion structure based on the results of SAXD, WAXD and DSC.

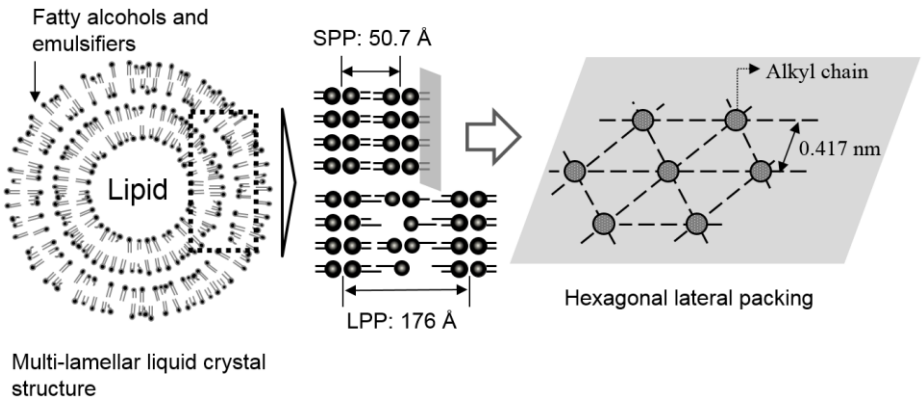

Evaluation of LC emulsion using MMP.

Comparison of the images obtained using MMP and a cryo-SEM. The LC emulsion and ordinary emulsion were evaluated using a cryo-SEM and an MMP. The principle of the MMP which was described by Arteaga et al. is shown in Figure 4.[19b] The polarized beam is reflected at the sample surface and the beam phase is changed when the sample structure is LC.

Figure 4. (a) Principle of polarization property evaluation with MMP (b) Schematics of Mueller matrix polarimeter (MMP) reprinted with permission from Axometrics.

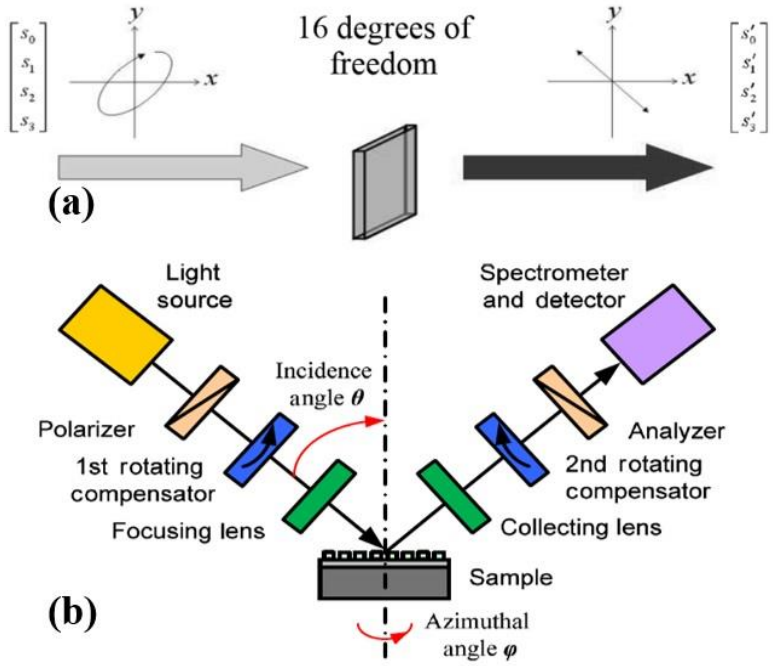

By calculating the retardance of reflected beam with the Mueller matrix equation, we estimated the polarization properties as a function of wavelength. In the calculation, the LC droplet can be considered as a composite of thin slices, which is a single birefringent element.[24] Because the retarders are generated from the single birefringent plate, the polarization properties show moderately linear correlation with the retardance of wavelength;[25] therefore the degree of polarization can be evaluated as a function of wavelength retardance, which is shown in Figure 5. The benefit of using MMP is the convenient evaluation of LC emulsions compared to cryo-SEM. Cryo-SEM is generally used to observe the LC structure; however, there are several limitations. First, preconditioning should be performed to prepare a sample such as lyophilization, during which the deformation of LC emulsions can occur. Second, the capturing images of emulsion droplets are so difficult even

in the freezing state that only an experienced analyst can obtain the appropriate image. In the case of using MMP, the LC image can be obtained without processing a sample and captured similarly as in the case of a general optical microscope.

Figure 5. (a) Images from cryo-SEM (up), Mueller matrix 2D (mid) and 3D (down); (b) Evaluation of the thickness and retardance of the polarized beam of LC material.

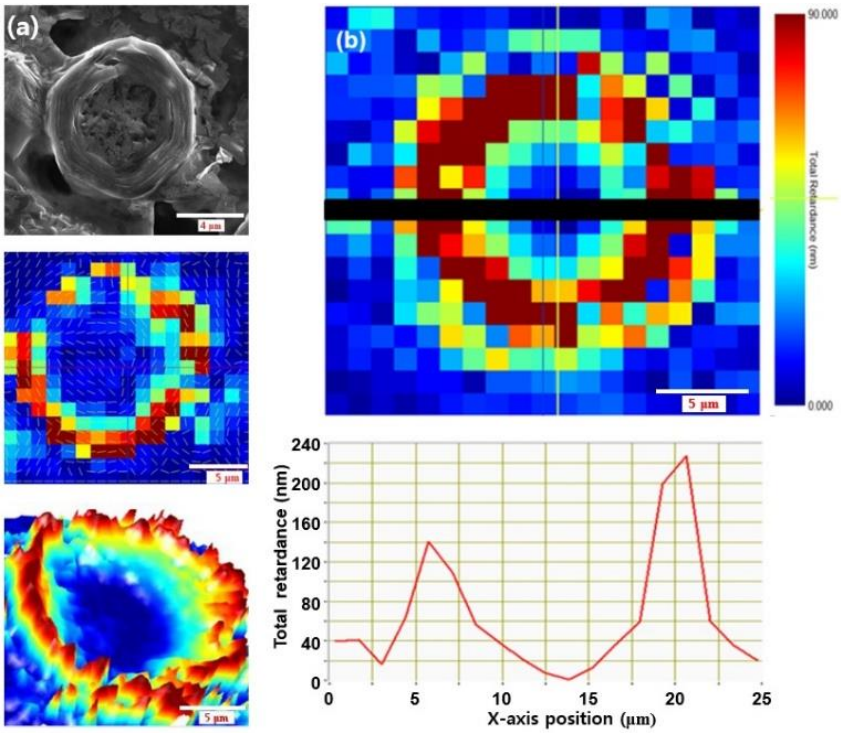

The cryo-SEM image of LC emulsion was compared to that of the MMP as shown in Figure 5(a). In the MMP image of LC emulsion, the phase transformation of the penetrated beam was consistent with the LC structure observed by cryo-SEM. The thickness of LC phase and wavelength retardance of polarized beam can be evaluated using MMP as shown in Figure 5(b). The thickness of the LC phase was ~5 µm. The peak of wavelength retardance was observed at the interphase (red colored) and the beam was not significantly

retarded at the inner and outer phases because of the isotropic structures of the phases (blue colored). The polarization of an *ex-vivo* human skin sample was evaluated with the same evaluation mode of LC emulsion to determine that SC was composed of the LC structure. The LC structure of emulsion can be regarded as a SC mimic because the reported image of the LC structure of SC was obtained by mixing the intercellular lipids isolated from SC and a certain amount of water.[26] Therefore, it is not a direct image of SC. The result of SC is shown in Figure 6, indicating that the wavelength retardance of polarized beam was estimated to be 18.894 nm. Therefore, it can be considered that the structure of SC exists as LC on the human skin.

Figure 6. MMP (a) and microscope (b) images of SC.

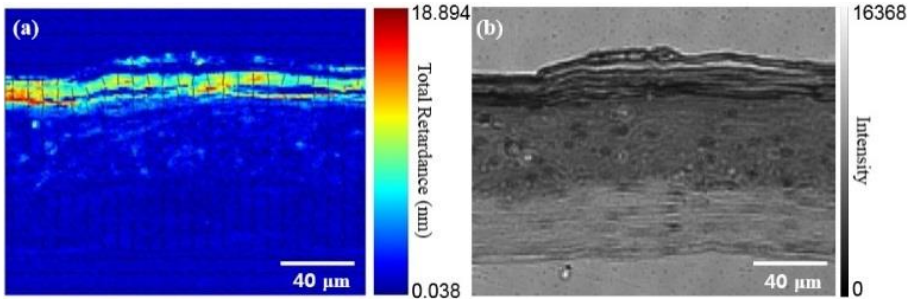

The isotropic and anisotropic properties of the ordinary emulsion and LC emulsion shown in Table 1 were evaluated using MMP. Only a blue zone was observed in the ordinary emulsion, while the LC phase in red was observed for LC emulsion as shown in Figure 7.

Figure 7. Comparison of the LC emulsion with the ordinary emulsion using MMP. The white bars correspond to 20 μm

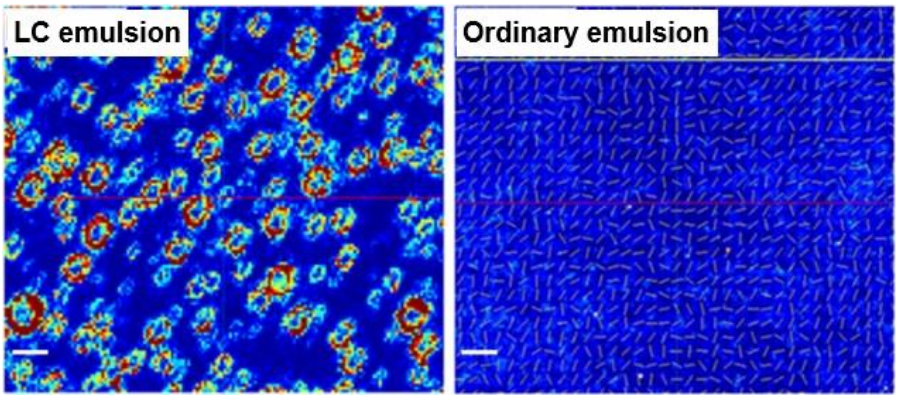

Evaluation of the stability of LC emulsions using MMP. The stability of LC emulsion with RP was evaluated using MMP in free-thaw, under 4 ℃, and 45 ℃ storage conditions for three months. The anisotropic peaks of LC emulsion with RP were 140 and 230 nm at 1 d after the preparation, and the values were checked at 1, 2, 4, 8, and 12 weeks and compared with the ordinary emulsion with RP prepared without C12–20 alkyl glucoside. As shown in Figure 8, the retardance of the sample stored at 45 ℃ for 12 weeks was comparable to that of the standard sample stored at 25 ℃ for the same period; thus, the LC structure of emulsion did not change under the accelerated conditions of deformation of the LC structure, resulting from fatty alcohol migration and rearrangement. A plausible mechanism for the preservation of LC emulsion structure, linked with the results of DSC, involves the prevention of fatty alcohol swelling with C12–20 alkyl glucoside due to numerous hydroxyl groups within the glucoside.[27] The swelling of the LC phase can be attributed to the increase in water molecules at the inter-lamellar structure. As water molecules penetrate the structure, the emulsion droplets grow larger because of the increased thickness of the LC phase. The stronger the hydrogen bonds of fatty alcohols or emulsifiers at the inter-lamellar structure, the poorer the penetration of water molecules. Because the glucoside has more polar head groups, it can form more hydrogen bonds with

the adjoining LC layer; therefore, the L_α phase in LC emulsion can exist at higher temperature than that in ordinary emulsion, as described in the results of DSC, which is resistant to the swelling effect. Because the LC emulsion after swelling is unstable because of the droplet size increase and coalescence, the swelling delay is the key to improve the stability of LC emulsion.[28]

Figure 8. Stability assessment of LC emulsion incorporated with RP using MMP; MMP images of the LC emulsion with RP stored at 25 ℃ a) and 45 ℃ for 12 weeks (b). The average retardance of polarized beam with LC emulsion with RP kept at 45 ℃ was not statistically different from that at RT (c). The white bars correspond to 20 μm (a and b).

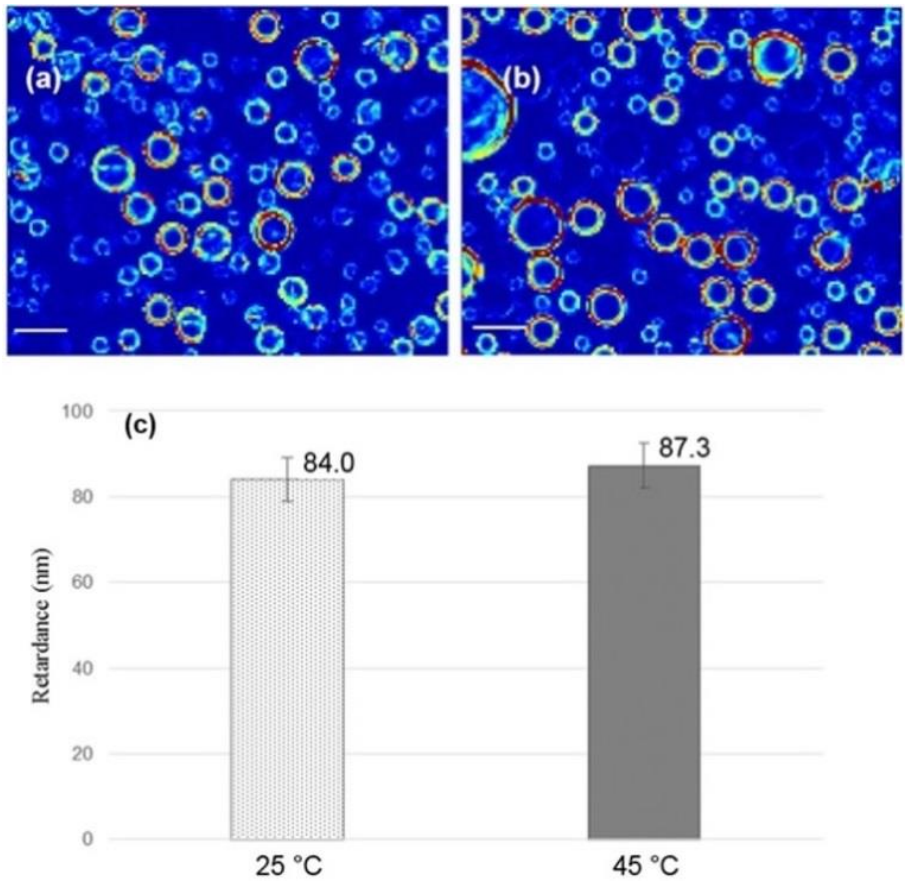

Enhanced penetration of RP on human skin with *in vivo* confocal Raman scattering microspectroscopy. To evaluate the efficacy of RP as a penetration promoter, the LC and the ordinary emulsion incorporated with RP were evaluated with confocal Raman spectroscopy. In confocal Raman spectroscopy, the frequency of RP appeared at 1162, 1194 and 1596 cm^{-1} as shown in Figure 9.

Figure 9. Spectrum of the LC emulsion without RP (a) and with RP (b) in confocal Raman spectroscopy. The different peaks of the emulsion with RP are 1162, 1194 and 1596 cm^{-1}.

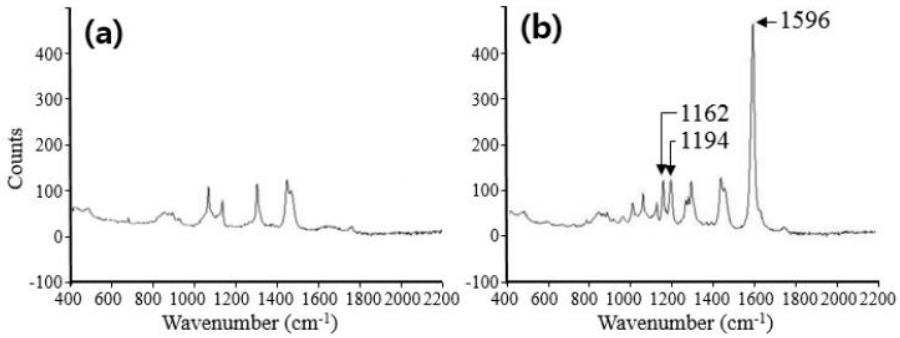

The band from RP at 1596 cm^{-1} is related with the common chemical structure of retinol, carbon-carbon double bonds, because the band is comparable with the known Raman bands of carbon-carbon double bonds, around 1600 cm^{-1}, and almost identical with the one from retinol at 1594 cm^{-1} as reported by Pudney et al.[21] The intensities of 1596 cm^{-1} were relatively strong compared to those of the other ingredients in both the LC and ordinary emulsion, therefore the evaluation of RP permeation was performed with the signal at 1596 cm^{-1}. The quantities of RP penetrating the skin were evaluated at every 2-μm depth and the quantities of penetrated RP were calculated by the summation of the values at every 2 μm from the skin surface to 24 μm depth and the values are presented in Figure 10.

Figure 10. Dermal delivery of RP incorporated into the LC emulsion (a) and the ordinary emulsion (b) in the randomized *in vivo* trial. Two separate measurements per subject were performed with random application of the LC emulsion to one of volar forearms of the subject and the ordinary emulsion to another one of the subject. The estimation was repeated within the same site and ten scans were collected for each scheduled intervals. The results are shown as an arbitrary unit which is the contents of RP relative to the amount of keratin, which is processed using the built-in analysis software, SkinTools v2.0 (River Diagnostics).

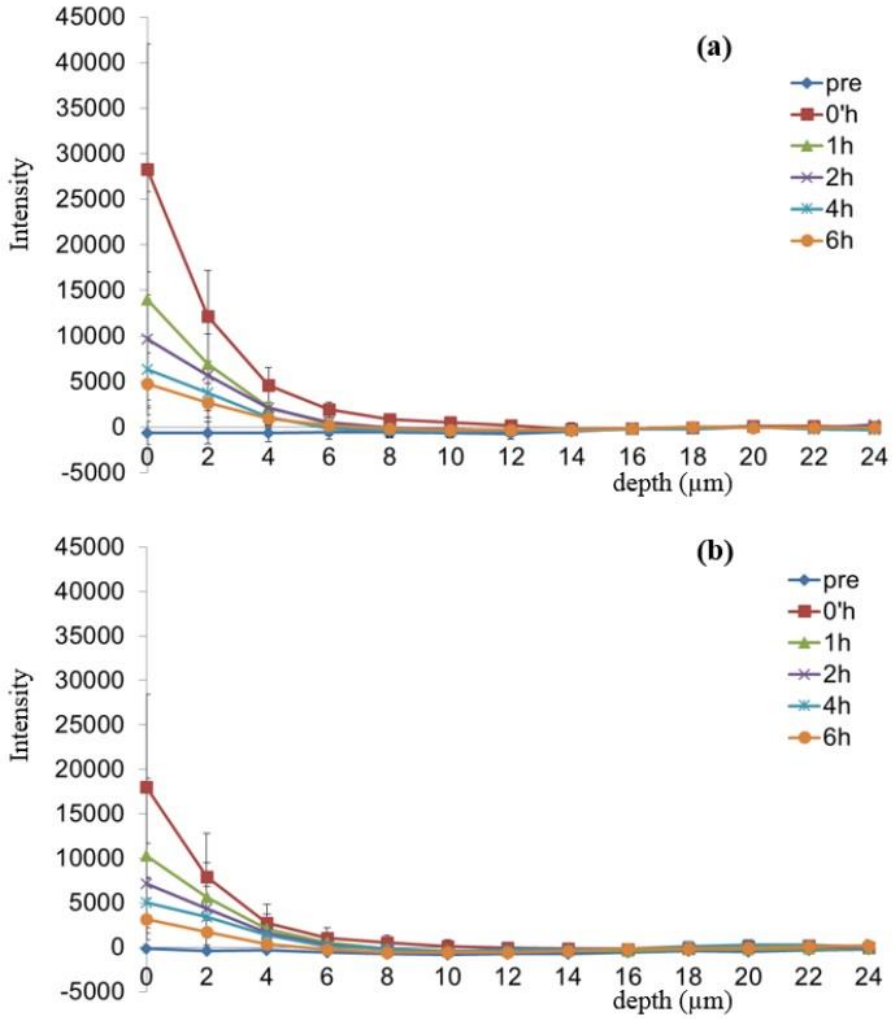

The collected signals became weaker as the probe went deeper into the subject not because of the loss of compound but because of the light scattering increase.[21] As shown in Figure 10, there is a significant effect in the dermal delivery of RP with the LC emulsion compared to the one with an ordinary emulsion. The signal intensity values of RP with the LC emulsion were 28,300, 12,200, 4,630 and 1,910 A.U. for 0, 2, 4 and 6 μm depths at 0`h, respectively, which are 56.6%, 54.0%, 68.6% and 82.4% higher than those with the ordinary emulsion, 18,100, 7,920, 2,740 and 1,050 A.U. for 0, 2, 4 and 6 μm depths at 0`h, respectively ($p < 0.05$). Because the reduction in RP may indicate that the RP penetrated into deeper layer of epidermis as reported by Pudney et al.,[21] the penetration values of RP into epidermis were calculated by subtracting the values at 1, 2, 4 and 6 h from the one at 0`h as described in Table 2. For example, the reduction of RP value at 1 h, 24,500 A.U., was calculated by subtracting the value at 1 h, 23,400 A.U., from the one at 0'h, 47,900 A.U. in the evaluation of LC emulsion. The value reductions of RP incorporated into LC emulsion were 24,500, 30,100, 37,300 and 39,500 A.U. at 1, 2, 4 and 6 h, respectively, while the reductions of the ordinary emulsion were 11,900, 17,100, 20,700 and 25,800 A.U. at 1, 2, 4 and 6 h, respectively. Thus, the enhancement in RP permeation with LC emulsion can be calculated as 106%, 76.0%, 80.2% and 53.1% at 1, 2, 4 and 6 h, respectively, and the differences were statistically significant with 95% confidence. The mechanism of permeation enhancing can be postulated based upon previously reported studies of topical applications. First, the LC structure of SC can be disrupted by the LC structure of emulsion.[9d] Because the structure of emulsion is similar with that of SC, the fatty alcohols and surfactants in the LC phase of emulsion can interact with the intercellular lipids in the SC, leading to a more liquefied and permeable packing of lipids.[29] One of the disruption mechanisms of SC barrier function is the efficient hydration effect of LC emulsion.[30] The hydration efficacy of LC emulsion in topical application is greater than that of the ordinary emulsion. Therefore the inter-lamellar volume of lipid bilayers can be increased because the LC structure can change

with insertion of water molecules into the flexible layer of lamellar LC consisting of polar head groups.[31] As a result, the permeation of RP into SC can be promoted with the disorganization enhancement. Therefore, it can be concluded that the LC emulsion in this study is a more efficient dermal carrier of RP than the conventional emulsion.

Table 2. Sum of RP inside skin and reduction of RP at 1, 2, 4, and 6 h. The reduction is calculated by subtracting each value from the value at 0`h.

	Ordinary Emulsion				LC Emulsion			
	Sum of RP inside skin		Reduction of RP		Sum RP inside skin		Reduction of RP	
	Average	Standard deviation	Average	Standard deviation	Average	Standard deviation	Average	Standard deviation
0`h	30,300	18,100	-	-	47,900	21,200	-	-
1h	18,400	15,400	11,900	12,300	23,400	20,600	24,500	18,300
2h	13,200	8,630	17,100	12,100	17,800	16,200	30,100	15,200
4h	9,600	6,190	20,700	14,100	10,600	6,760	37,300	17,500
6h	4,500	4,920	25,800	16,900	8,400	6,840	39,500	14,500

III. Conclusion

The lamellar LC emulsions incorporated with C12–20 alkyl glucoside, fatty alcohols, hydrogenated lecithin, and other lipids were successfully prepared. In the formation of the LC structure, the type of surfactant was an important factor; well-arranged LC structures were obtained with an appropriate composition. The LC structures were evaluated by conventional methods such as polarized microscopy, cryo-SEM, DSC, SAXD, and WAXD and then compared with the results obtained using MMP. Notably, the preconditioning of sample was not required in the MMP method; therefore, the phase change during the evaluation or other transformation could be prevented. Besides, the test could be carried out in a very short time, i.e., within 20 s, while other evaluation methods such as cryo-SEM, DSC, SAXD and WAXD require several hours. The stability of the prepared LC emulsions was investigated using an MMP, and the retardance values of the polarized beam obtained after a three month test were comparable to the standard values. The stability improvement can be explained by the fact that the deformation of LC structure (L_{α}) could be delayed with the prolonged transition state observed between 37 and 60 ℃ with the maximum peak at 48 ℃. For the application of the prepared LC emulsions, the enhancement in RP penetration was evaluated by in vivo confocal Raman spectroscopy, and the sum of RP permeation values detected in selected skin depths using the LC emulsions was 106% higher than that of the ordinary emulsion. Therefore, the LC emulsions presented in this study are efficient biomaterials in topical applications as evidenced by the enhanced penetration of RP.

IV. Experimental

Materials

C12–20 alkyl glucoside (SEPPIC, France), sorbitan palmitate (Biologia & Tecnologia, Italy), ceramide-3 (Doosan, Korea), cholesterol (Nippon fine chemical, Japan), hydrogenated lecithin (Lipoid GmbH, Switzerland), PEG-100 stearate (Croda, USA), glycerine (Emery Oleochemicals, Malaysia), carbomer (Noveon, Canada), and stearic acid (Jeong Nam, Korea) were obtained from the commercial sources indicated. Glyceryl stearate, caprylic/capric triglyceride, 1-octadecanol, RP, dipropylene glycol, and 1-hexadecanol were purchased from BASF (Dusseldorf, Germany). All the materials were of analytical grade.

Sample preparation

The LC and ordinary emulsions were prepared by hot process emulsification. As described in Table 1, the ingredients of ordinary emulsions and LC emulsions are the same; except that PEG-100 stearate was applied in the ordinary emulsions while the alkyl glucoside and sorbitan palmitate were incorporated into LC emulsions, which function as promoters of LC structure formation. The ingredients shown in part A, Table 1, were dissolved at 80 ℃ and then added into the ingredients shown in part B, Table 1. The resulting mixture was homogenized using a T.K. Robomix (Primix, Japan) at 5,500 rpm for 5 min. The resulting emulsion was cooled down to 25 ℃ in 17 min with observing the formation of LC phase.

Sample monitoring using a microscope

The prepared LC emulsions were observed using a polarized microscope,

HVC-3000 PS (Hyvision, Korea), during the cooling process and stability tests. The microscope images were obtained using an image capturing software (HySCALER Version 1.4.0). The images of LC emulsions stored at 25, 4, 45, and 50 ℃ were compared with those of the standard samples for the stability assessment.

Small and wide-angle X-ray diffraction

The structures of the LC emulsions were characterized by SAXD and WAXD analyses using a D8 Discover with General Area Detector Diffraction System (GADDS, BRUKER, Germany) at National Instrumentation Center for Environmental Management, Seoul, Korea, and the generator was operated at 40 kV and 40 mA. The distance between sample and detector was 300 mm, and the exposure time was 1,800 sec. To obtain a narrow beam, a collimator with 0.2 mm size was used and the sample holder was the standard disc-shaped one with the fixed-chi stage at 54.74°. The SAXD and WAXD patterns were obtained using Hi-Star area detector, and the 2θ range was from 2 to 50° for every 0.02 step at 1 s/step scan speed. The distance between the planes of LC, d, was calculated from the obtained indexing peaks in the scattering patterns of SAXD using Bragg's equation, $n\lambda = 2d\sin\theta$, where λ is the wavelength of the X-rays (1.54226 Å) and θ is the angle of scattering. The calculated interplanar distance was multiplied by the peak ratio of the particular peak. The peak ratios for the Lα structure were 1, 2, 3, etc. The LC phase was also determined using WAXD by comparing the indexing peaks in the scattering patterns with the peaks of the reported LC structure of SC.

Differential scanning calorimeter

The thermal property of LC emulsions was investigated using a DSC-Q1000 (TA Instrument, UK) at the National Instrumentation Center for Environmental Management equipped with a thermal analysis data system for

the baseline correction, transition temperature, and calculation of the transition heat. Ordinary emulsion (6.10 mg) and LC emulsion (3.00 mg) were placed in aluminum hermetic pans, separately, and then cooled to 20 ℃ and then heated up to 80 ℃ at a heating rate of 2 ℃/min under a constant flow of nitrogen gas.

Cryogenic scanning electron microscope (cryo-SEM)

The samples were frozen at -190 ℃, and all the samples were kept in a freezer before lyophilization. The emulsions were freeze-dried for 5 d using a freeze dryer (ALTO-2500, TATAN, UK) at 25 ℃ in the drying chamber, -190 ℃ in the cooling unit, and in a vacuum of 10^{-3} mbar. The lyophilized samples were transferred to the preconditioning chamber and cut into thin pieces. The obtained sliced samples were coated with Pt/Pd at 10 mA for 120 s. The freeze-fracture cryo-SEM of sliced LC emulsions was analyzed using a Quanta 3D FIB (FEI, The Netherlands) operated at 5 kV and a working distance of 9.9 mm.

Mueller matrix polarimeter

The optical system of AxoStep (MMISP, Axometrics, USA) is composed of a polarizer, analyzer, rotating retardation film, and microscope, and the values can be measured as rotational retardations by calculation using built-in analysis software based on Mueller matrix method. The polarization-state generator consists of a laser diode, polarizer, 1st rotating compensator, and focusing lens that keeps the polarized light at 45°. The laser light was focused to a 70 μm diameter spot on the sample surface with the polarization state configured by the computational controlled LC retarders of AxoStep. The polarized beam was reflected at the sample surface and the polarization-state analyzer consisting of a collecting lens, a 2nd rotating compensator, an analyzer, and a spectrometer provided the image. For the evaluation of SC

structure, ex-vivo human skin samples were measured in the same evaluation mode described above.

In-vivo confocal Raman microspectroscopy

The Raman measurements were performed using a skin composition analyzer (Model 3510 SCA, River Diagnostics, Rotterdam, Netherlands), which comprises a built-in optical module and an inverted microscope optimized for the near infra-red wavelength, two lasers operating at 785 and 671 nm, and a control software (RiverlCon, River Diagnostics, Rotterdam, Netherlands, http://www.riverd.com/model3510.html). For the measurement, the axial spatial resolution was 5 µm, the spectral resolution was 4 cm^{-1}, and the laser excitation wavelength was set at 785 nm. The setup was employed to estimate signals of unknown chemicals. The volar forearm of the subject was placed on a fused silica window used at the measurement stage. Laser light was focused on the skin with a microscope objective located under the window and the microscope objective was immersed in oil to minimize the error associated with sampling depth, which allows accurate measurement of the Raman microspectroscopy.[21, 32] The Raman fingerprint spectra (400–2000 cm^{-1}) were recorded from the skin surface down to a depth of 24 µm in 2-µm steps. For each spectrum, the exposure time was 5 s. After each measurement, the laser was positioned on a different skin area within the same site, and the measurements were repeated. Ten scans were collected for each treatment site at pre-treatment, 0`h (0.5 h), 1 h, 2 h, 4 h and 6 h. The collected data were calibrated and corrected for the analyzer response using SkinTools v2.0 (River Diagnostics, Rotterdam, Netherlands), which is a built-in software for analysis equipped with a built-in database of spectra of skin constituents and an automated fitting algorithm. Briefly, the calibration with the built in software was performed by normalizing of all spectra obtained at the measurement to the keratin signal to compensate for the signal attenuation by the absorbance and scattering increase with depth into the skin.[33] After acquiring of the

normalized spectra, the spectra were fitted by applying the fitting model based on the component of skin, which is a multiple least squares fit algorithm.[20] Therefore, the contribution of specific molecules can be measured with the model. The content of RP was calibrated with the relative intensity to that of keratin, as arbitrary unit (A.U), in order to compensate the physical effect.[21] Therefore the value means the contents of RP relative to the amount of keratin. This method is suitable because the purpose of study is to evaluate the relative performance of dermal delivery system comprising LC emulsion compared to the other systems comprising ordinary emulsion.

***In-vivo* confocal Raman microspectroscopy - Protocol**

The topical delivery experiments were performed on the volar forearms of five female subjects with age ranging from 35 to 40 years under standardized conditions. The experiments were conducted according to the Good Clinical Practices guidelines and regulations on the Human Study of Health & Functional Food from the Ministry of Food and Drug Safety in Korea and permitted by the institutional review board of Department of Genetic Engineering & Skin Biotechnology Center in Kyung Hee University, which is certified by the Korea Centers for Disease Control and Prevention. The volunteer's willingness to participate in the study was confirmed by means of written informed consent. The subjects cleaned their volar forearms and took rest for at least 20 min in a space where constant temperature and humidity (22 ± 2 ℃, 50 ± 5 %) were maintained without air flow and direct light to prepare for the evaluation. Prior to the applications of products, 4 × 5 cm^2 measurement areas (volar forearm) were marked and measured. Then, the areas were treated with 300 mg of the LC emulsion on one site of the volar forearm and the ordinary emulsion on another site of the subject. The application site of the product was determined randomly as the left or right volar forearm of the subject to minimize inter-personal variation. The measurements started 30 min after the product application on the volar

forearm skin. The Raman spectra were collected from the skin surface to 24 μm below with 2-μm steps and ten scans were collected for each treatment site at each time point for 20 min. The baselines were measured after treating the sites with the LC emulsion or ordinary emulsion without RP. The RP contents in the skin were measured at the baseline and immediately after the application (30 min application), as well as 1, 2, 4 and 6 h after the application of the product.

Part II.

Liquid crystal nanoparticle formulation as an oral drug delivery system for liver-specific distribution

I. Introduction

In recent years, hydrophobic peptide-based therapeutics have been investigated intensively owing to their many benefits compared with low molecular weight drugs.[1] These benefits include extremely high potency achieved from structure-based drug design, selectivity, broad spectrum of application, lower toxicity, vast chemical and biological diversity, and ease of discovery at the peptide and nucleic acid levels.[1-2] Although many hydrophobic peptide-based therapeutics have been developed, most of them have shortcomings, such as poor metabolic stability, poor oral bioavailability, rapid clearance, and poor solubility.[3] To overcome these obstacles, new drug delivery systems have been intensively studied during the last decade and many successful results have been reported. These systems include liposomes,[4] PEGylated (polyethylene glycosylated) peptides,[5] lipid nanocapsules,[6] solid lipid nanoparticles,[7] liquid crystal nanoparticles (LCNPs),[8] and polymeric nanocapsules.[9] Many hydrophobic peptide-based therapeutics have been approved on account of the new drug delivery systems. However, there are still unresolved challenges related to some persistent drawbacks, including the instability of vesicles for liposome and lipid nanocapsules,[10] as well as the limited application of PEGylation.[5a]

Among the reported drug delivery systems, LCNPs have received increasing attention because of the advantages they offer compared to other systems. For example, LCNPs are often incorporated with biocompatible and non-toxic excipients compared to polymeric nanoparticles; hence, oral delivery of LCNPs is possible.[11] In a similar fashion to the protection afforded to the biodegradable drugs by polymeric nanoparticles, the liquid crystalline structure of LCNPs can protect active ingredients from the harsh gastrointestinal conditions.[12] Additionally, sustained drug release may be

achieved with drugs incorporated in LCNPs,[13] allowing for a reduction in drug toxicity, which can be elevated at high drug concentrations.[14] However, LCNPs have not been widely applied, particularly owing to the high costs associated with the massive energy input required in the manufacturing process, which includes high-shear homogenization and high-pressure emulsification or ultrasonication.[8, 15] Since the introduction of lipid nanocapsules with the phase inversion temperature (PIT) method,[16] numerous topical, oral, and pulmonary applications of the nanocapsules have been implemented.[17] The benefits of the PIT method include low energy and cost inputs, short realization time, obviation of organic solvents, and versatile application for lipophilic drugs. The lipid nanocapsules can also circumvent a number of drawbacks associated with conventional drug delivery systems.[16c] In addition, these nanocapsules improve drug bioavailability and drug stabilization, and the PEGylation of the particle surface prevents interaction with serum components, which allows for improved pharmacokinetic (PK) profile and prolonged residence time.[18] However, it has been challenging to ensure that the capsules are stable against flocculation, which leads to an increase in vesicle sizes and emulsion instability.[19] From our studies on the lipid nanocapsules prepared with the PIT method, we hypothesized that the preparation of LCNPs using the PIT method could be a solution to these limitations because particle aggregation can be prevented by the liquid crystal structure of LCNPs, which is stabilized by the bulky chains of the surfactants.[20] Moreover, we envisioned that the LCNPs could be used as a liver-specific delivery system, avoiding clearance by the mononuclear phagocyte system, because the surface of the LCNPs is covered with the PEG chains and the size of the LCNPs can be set to around 100 nm.[21]

In this study, we report a novel and economic drug delivery system using LCNPs prepared by the PIT method incorporating a new hepatitis C virus

(HCV) NS5A inhibitor, BMK-20113. BMK-20113 is a very hydrophobic peptide-based drug candidate possessing an excessively high inhibitory activity against the protein (half maximal effective concentration, EC_{50} = 0.26 nM).[22] However, it exhibited a rather undesirable PK profile in rats.[22] The composition of LCNPs incorporating BMK-20113 and the manufacturing process were optimized by varying the quantities/proportions of surfactants to melting lipids and then observing the phase behavior at the PIT of the complex. The physicochemical properties of the LCNPs were evaluated using conventional methods, including small- and wide-angle X-ray diffraction (SAXD and WAXD), particle size analysis, differential scanning calorimetry (DSC), and transmission electron microscopy (TEM). The PK profiles and tissue distribution of BMK-20113 incorporated into the LCNPs were compared with those obtained from the examination of the compound incorporated in a conventional host–guest complex (HGC), which was previously utilized in PK studies of BMK-20113.[22]

II. Results

Preparation and physicochemical properties of LCNPs

The estimated PIT values and appearances of the LCNPs prepared with varying compositions are shown in Table 1. The ratio of Emulgade® SE-PF to PEG-12 cetostearyl ether was optimized by varying the ratio of the surfactant to the fixed concentrations of the surfactant mixture (10 wt%) and tetradecyl tetradecanoate (10 wt%). Semi-transparent dispersions were evident when the ratios of Emulgade SE-PF and PEG-12 cetostearyl ether were in the range of 2:1–2:3 and the phase inversion of the compositions appeared above 80℃. Based on previous reports that the stability of the formulation was improved as the PIT increased, a 1:1 ratio of Emulgade SE-PF and PEG-12 cetostearyl ether, which showed the highest PIT, was selected.[16b]

Table 1. Preparation of LCNPs

Entry (LCNP-#)	Composition				Results	
	Part A (wt%)			Part B (wt%)		
	Emulgade SE-PF	PEG-12 cetostearyl ether	Tetradecyl tetradecanoate	Water	PIT (℃)	Appearance
1	10.00	0.00	10.00	80.00	-	Separated
2	8.00	2.00	10.00	80.00	-	Macroemulsion
3	6.00	4.00	10.00	80.00	73	Transparent
4	5.00	5.00	10.00	80.00	83	Transparent
5	4.00	6.00	10.00	80.00	83	Transparent
6	2.00	8.00	10.00	80.00	93	Macroemulsion
7	0.00	10.00	10.00	80.00	98	Macroemulsion

Notes: Compositions, phase inversion temperatures, and appearances of liquid crystal nanoparticles.

Abbreviations: LCNPs, liquid crystal nanoparticles; PEG-12, polyethylene glycol-12; PIT, phase inversion temperature.

As the composition of surfactant mix, tetradecyl tetradecanoate and water was varied, semi-transparent nanodispersions were obtained at ratios of the dotted area illustrated in Figure 1. The dispersion with composition #8 in Figure 1 and Table 2 (LCNP-#8) was selected for further evaluation because it was incorporated with the highest amount of the lipid mix (30 wt% to the dispersion) comprising tetadecyl tetradecanoate (15 wt%) and the surfactant mix (15 wt%) compared with the other dispersions.

Figure 1. Ternary phase diagram of the surfactant complex, tetradecyl tetradecanoate, and water. The dotted triangle indicates the compositions at which the liquid crystal nanoparticles (LCNPs) can be prepared. The composition of LCNP-#8 is designated by a dark dot (•).

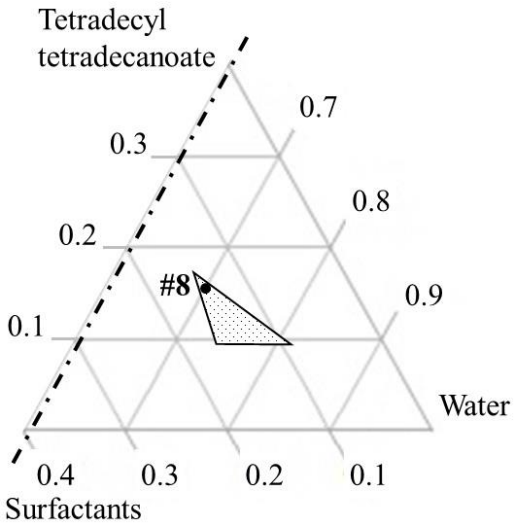

The phase behavior of dispersion LCNP-#8 on heating is described in Figure 2 with the estimation of electric current value. The electric current value decreased from around 140 μS at 80°C to below 20 μS at 95°C; hence, the

PIT was determined as 88℃, which is the median value of 80℃ and 95℃.[16b] BMK-20113 was incorporated in LCNP-#8 at 0.500, 1.50, 2.50, and 5.00 wt% to the lipid complex, as illustrated in Table 2. The 2.50 wt% sample of LCNP-#11 was selected for further PK studies because precipitation was observed with the 5.00 wt% sample (LCNP-#12). Drug stability during the heating process was evaluated using high-performance liquid chromatography (HPLC), and no drug decomposition was observed, as shown in Figure 3. BMK-20113 is practically insoluble in water[22] and is therefore assumed to be partitioned in the lipid phase of the LCNP dispersion.

Figure 2. Conductivity of liquid crystal nanoparticles (LCNP)-#8 on heating. A semi-transparent phase appeared as the conductivity decreased from 80℃.

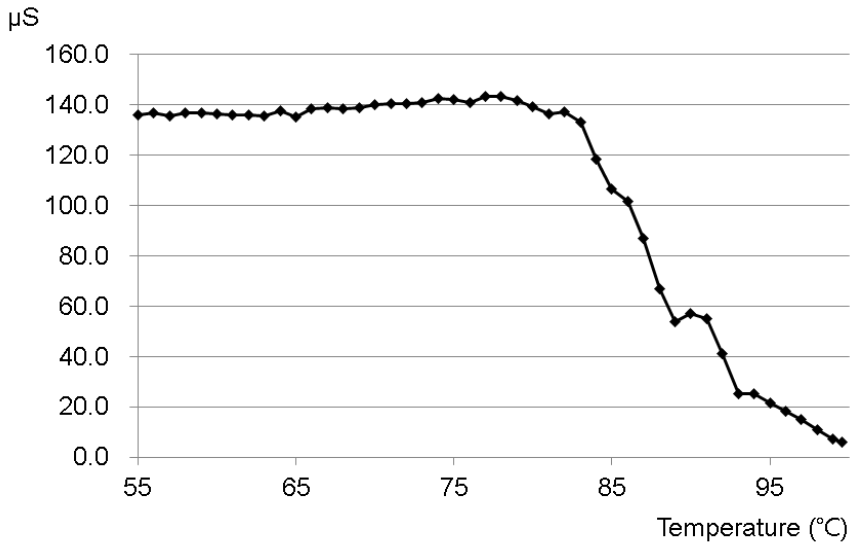

Figure 3. HPLC analysis of BMK-20113 incorporated into the liquid crystal nanoparticle (LCNP); (a) BMK-20113 in tetrahydrofuran, (b) LCNP-#8 and (c) LCNP-#11.

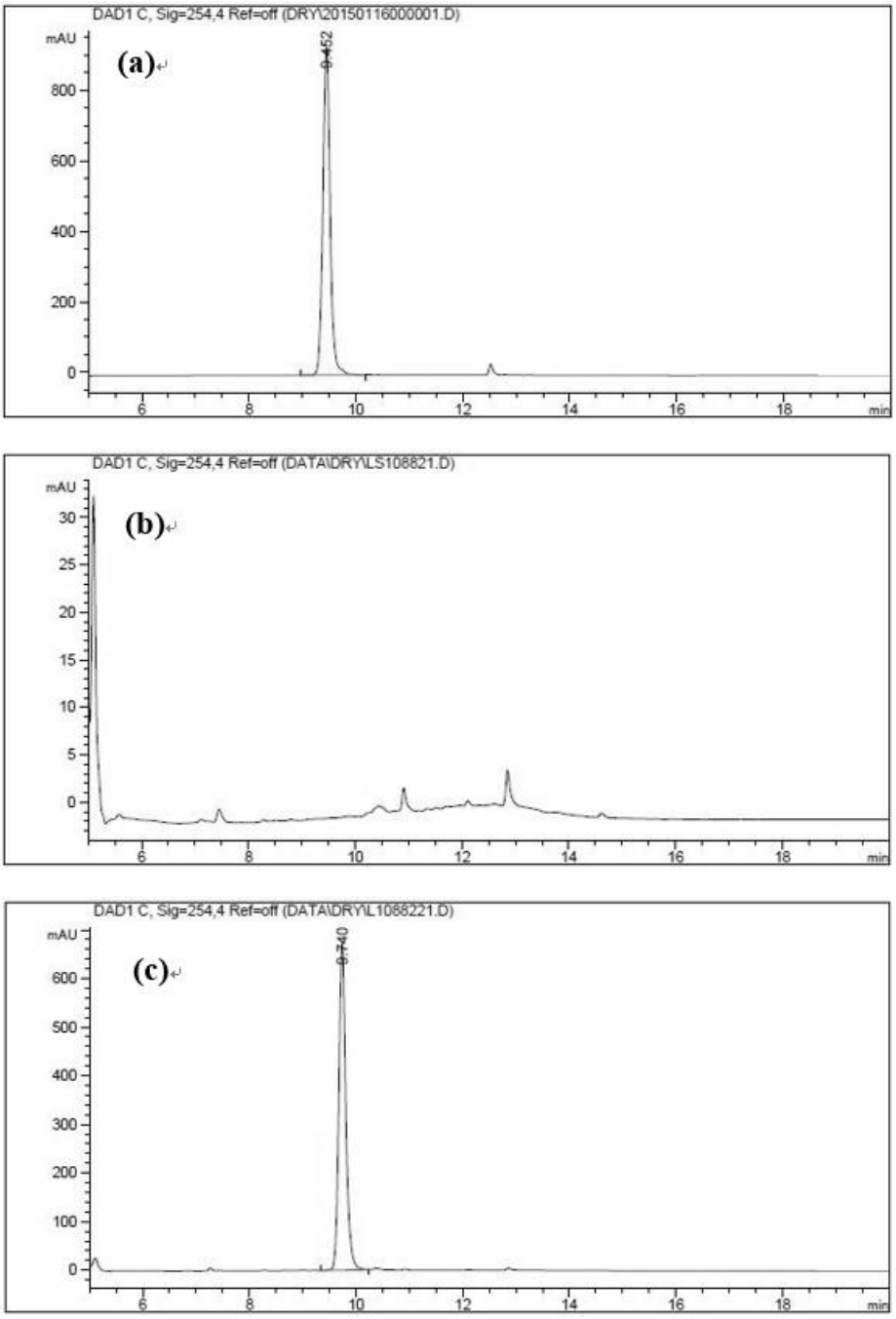

Table 2. Compositions of LCNPs for the pharmacokinetic study.

Ingredient	LCNP				
	#8	#9	#10	#11	#12
Water (g)	14.000	14.000	14.000	14.000	14.000
Emulgade SE-PF (g)	1.500	1.493	1.478	1.463	1.425
PEG-12 cetostearyl ether (g)	1.500	1.493	1.478	1.463	1.425
Tetradecyl tetradecanoate (g)	3.000	2.985	2.955	2.925	2.850
BMK-20113 (g)	0	0.0300	0.0900	0.1500	0.3000
BMK-20113 (wt% to lipid)	0%	0.500%	1.50%	2.50%	5.00%
BMK-20113 (wt% to dispersion)	0%	0.150%	0.450%	0.750%	1.50%

Abbreviations: LCNPs, liquid crystal nanoparticles; PEG-12, polyethylene glycol-12

The SAXD intensity (y-axis) is plotted against the scattering vector (x-axis) in Figure 4(a). Since the diffraction patterns are composed of sequential peaks, the LCNPs can be considered to have a lamellar liquid crystal structure. There is a correlation between the peaks positioned at 0.65 and 1.3 (nm^{-1}) with $2Q_1 = Q_2$, where *Q1* stands for 0.65 and *Q2* stands for 1.3. Therefore, the distance between the two phases is calculated to be approximately 9.7 nm by using Bragg's equation, $d = 2\pi/q$. From the results of the SAXD, it can be assumed that the surface of the LCNPs comprises a lipid lamellar phase with a periodicity of 9.7 nm. As shown in Figure 4(b), the scattering vector values in the WAXD are 15.0 and 16.6 (nm^{-1}); therefore, the distances between the hydrocarbon chains are 0.419 and 0.379 nm, respectively, according to Bragg's equation. These values are comparable with the orthorhombic lateral packing values, which are 0.41 and 0.37 nm, respectively, as reported by Bouwstra *et al.*[23] There were no differences in the distance values as the

concentration of BMK-20113 increased from 0 to 5.00 wt% in the lipid phase. From the results of SAXD and WAXD, it can be presumed that the LCNPs are composed of a lipid lamellar liquid crystal with orthorhombic lateral packing, as shown in Figure 5.

Figure 4. Evaluation of the physicochemical properties of the liquid crystal nanoparticles (LCNPs); (a) small angle x-ray diffraction (SAXD) and (b) wide angle x-ray diffraction (WAXD) of LCNP-#8, #9, #10, and #11. The lamellar liquid crystal structure is indicated by the sequential peaks positioned at 0.65 and 1.3 (nm^{-1}) in the SAXD. In the WAXD, the peaks positioned at 15.0 and 16.6 (nm^{-1}) correspond to the orthorhombic lateral packing structure. No significant changes were observed with varying concentrations of BMK-20113.

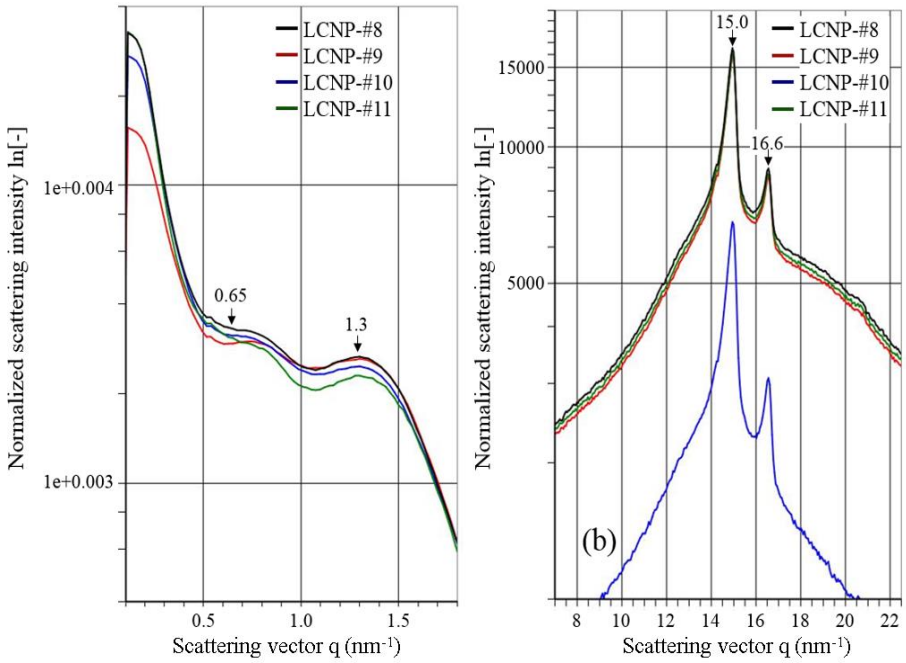

Figure 5. Illustration of the structure of the prepared liquid crystal nanoparticles (LCNPs). The interphase of the LCNPs is comprised of a lamellar liquid crystal structure with orthorhombic lateral packing.

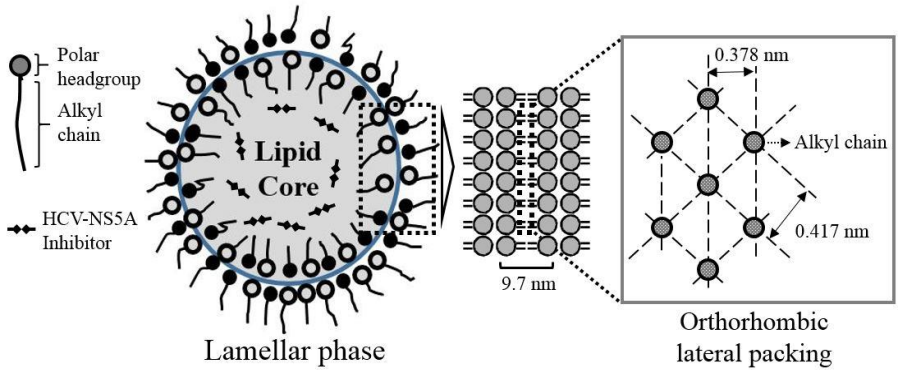

The DSC results are shown in Figure 6. The melting peak of the LCNPs without BMK-20113 was observed at around 35 ℃, which is lower than those observed for tetradecyl tetradecanoate (43.79℃), Emulgade SE PF (39.21℃) and PEG-12 cetostearyl ether (38.27℃), as shown in Figure 7. The enthalpy values of the LCNPs incorporated with 0, 0.50, 1.50, and 2.50 wt% BMK-20113 to the lipid mix were estimated to be 34.3, 34.3, 34.0, and 34.1 J/g, respectively.

Figure 6. The differential scanning calorimetry (DSC) curves for liquid crystal nanoparticles (LCNP)-#8, #9, #10, and #11. The main peaks from 33 to 36℃ and the small peaks at 25 and 32℃ for LCNP-#8 did not change significantly with increasing concentrations of BMK-20113.

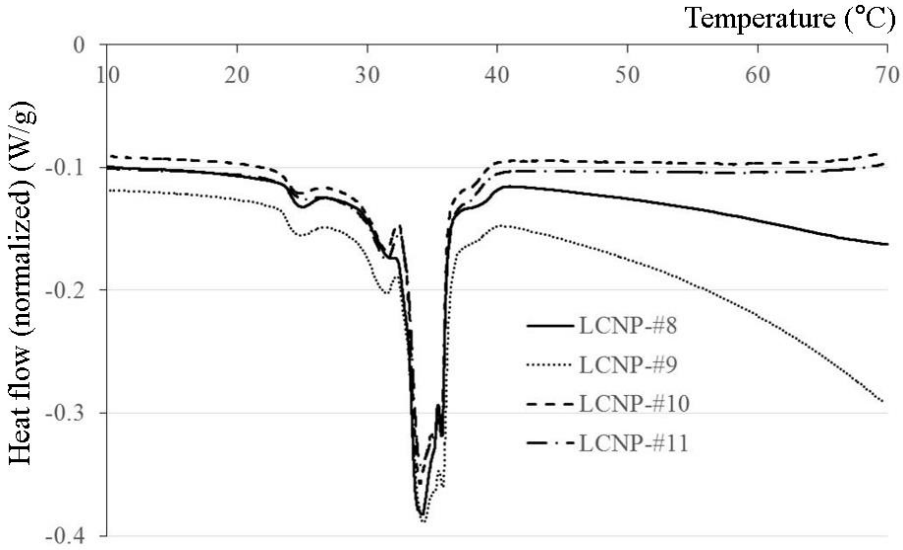

Figure 7. The differential scanning calorimetry (DSC) results of Emulgade SE-PF (a), tetradecyl tetradecanoate (b) and PEG-12 cetostearyl ether (c).

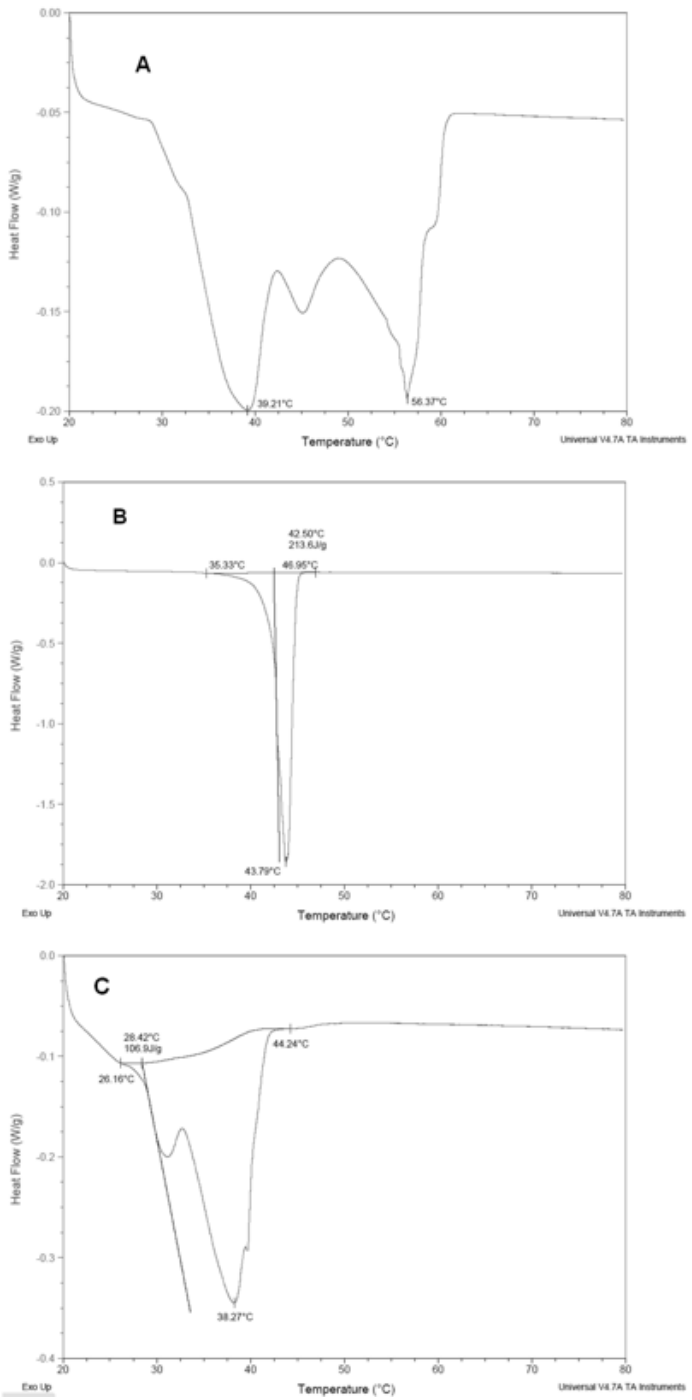

TEM images of the LCNPs incorporating BMK-20113 in 0, 0.50, 1.50, and 2.50 wt% to the lipid mix are shown in Figure 8. The sizes of LCNPs are from 70 to 130 nm and there were no significant differences in the particle shape at all tested concentrations of BMK-20113. However, the particle size increased with increasing concentrations of BMK-20113 from 0 to 2.50 wt%. There was no drug expulsion based on the TEM evaluation, which detects the drug recrystallization as shown in Figure 9. Additionally, the shapes and sizes of LCNP-#8 and #11 in an acidic condition (pH 1.5) were evaluated with TEM to ensure the stability in PO. As it is shown at Figure 10, the morphological properties of LCNP-#8 and #11 in the acidic condition were comparable with those of LCNP-#8 and #11 in the neutral condition.

Figure 8. Transmission electron microscopy (TEM) images of liquid crystal nanoparticles (LCNP)-#8, #9, #10, and #11.

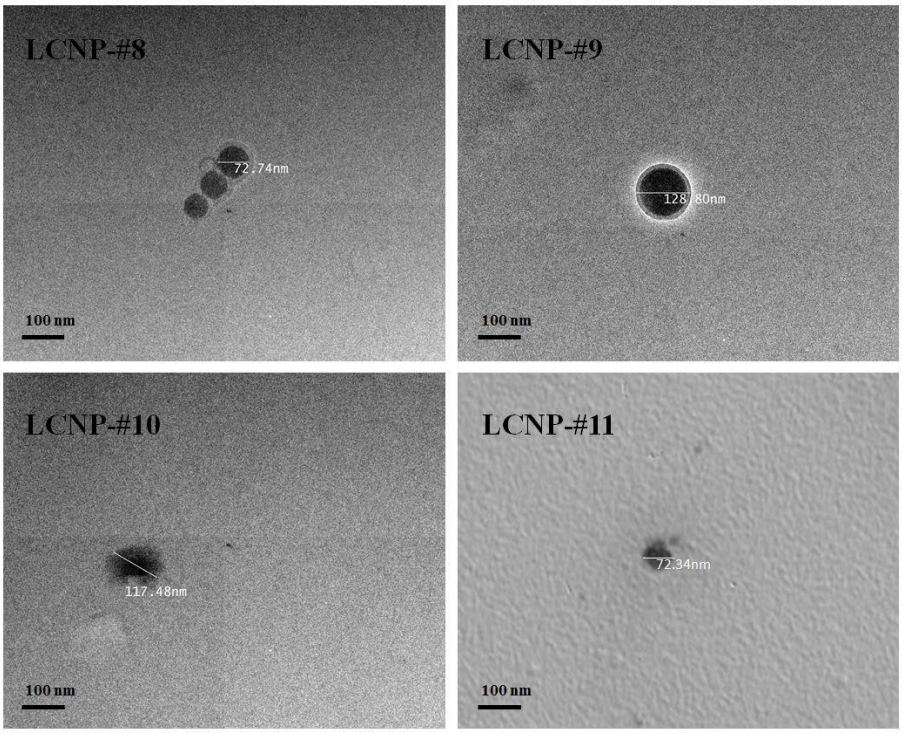

Figure 9. Transmission Electron Microscopy (TEM) image of BMK-20113 recrystallization of LCNP-#12.

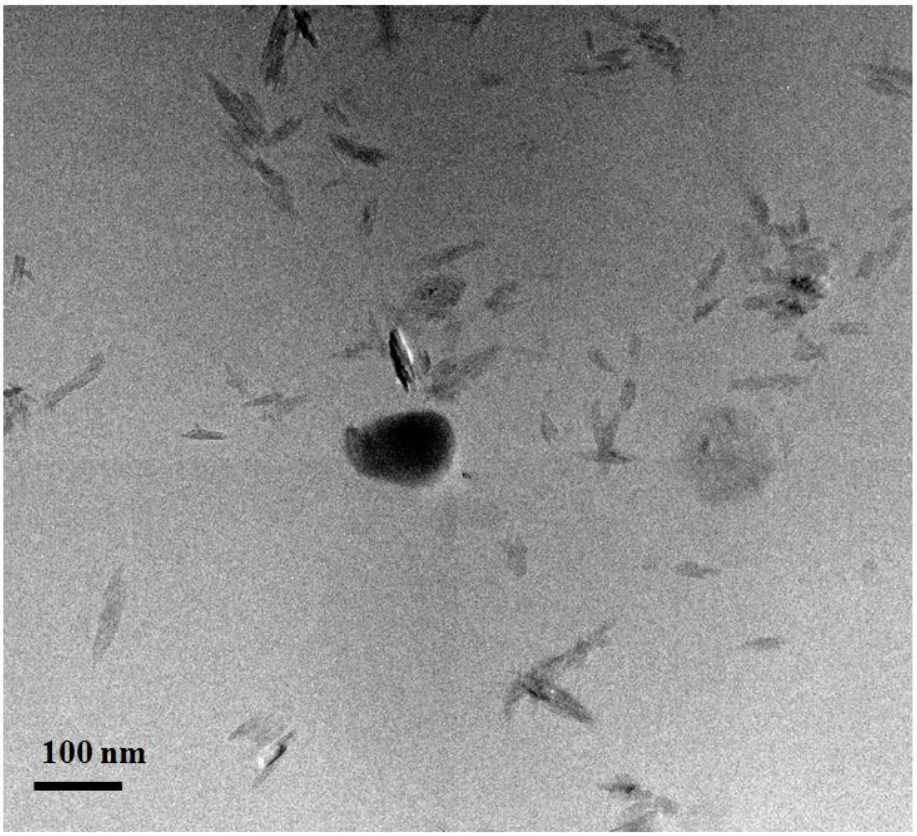

Figure 10. Transmission Electron Microscopy (TEM) image of LCNP-#8 and #11 in an acidic condition (pH 1.5)

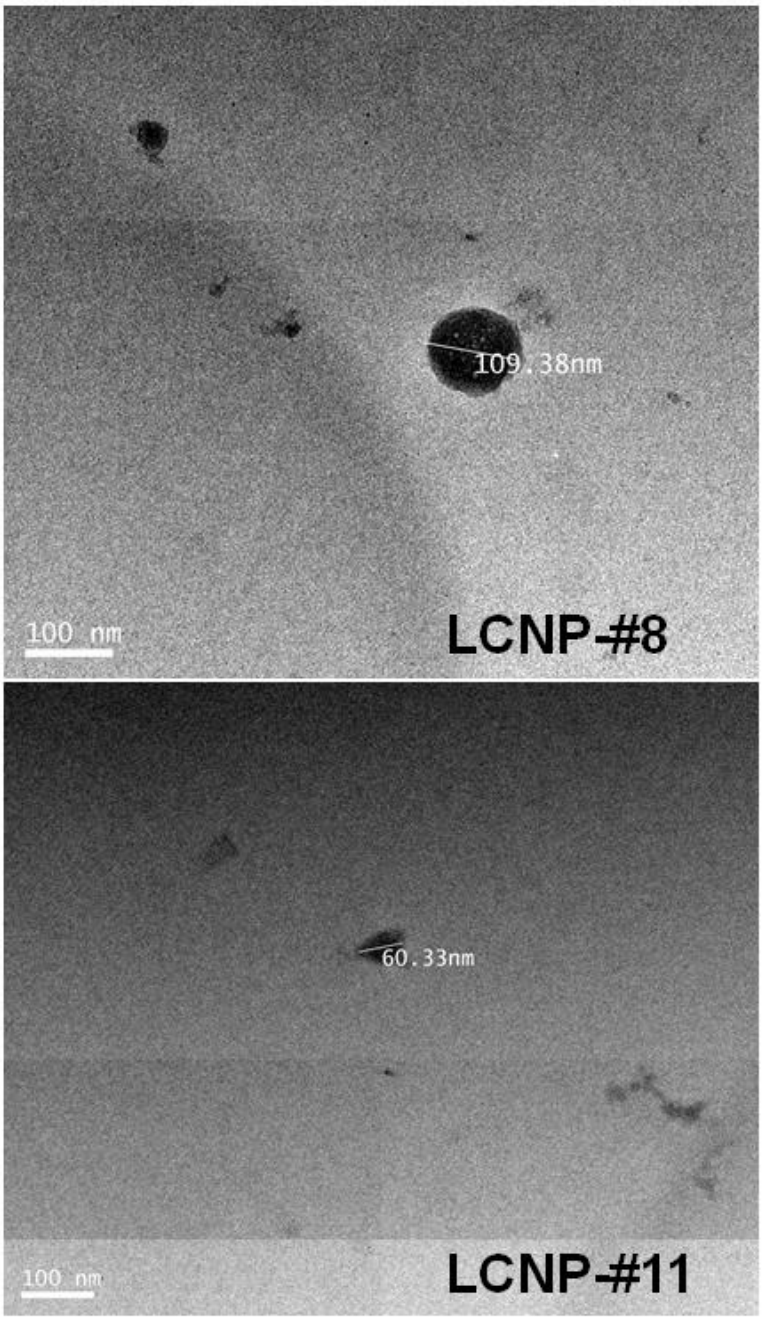

To evaluate the stability of the LCNP dispersions, particle size analysis was performed using dynamic light scattering at scheduled time intervals, and the results are illustrated in Figure 11. There were no significant changes in the particle size when stored at 4℃ from day 1 after preparation for up to 2 months. However, the particle size of the LCNPs with 2.50 wt% BMK-20113 was larger than that with other concentrations. At 37℃, there was no increase in the particle size at 0 and 0.50 wt% BMK-20113. However, a significant increase in size was observed in the LCNPs with 2.50 wt% BMK-20113 after 2 weeks. The LCNPs with 1.50 wt% BMK-20113 showed a slight increase in size after 2 weeks. However, this was comparable with the values at 1 and 2 months. This result suggests that the size increase is not accelerated until after 2 months.

Figure 11. Stability of liquid crystal nanoparticles (LCNP)-#8, #9, #10, and #11 at (a) 4℃ and (b) 37℃. LCNP-#8 and #9 are stable at 4℃ and 37℃ for 2 months, while LCNP-#10 and #11 are stable at 4℃ for 2 months and at 37℃ for 1 week.

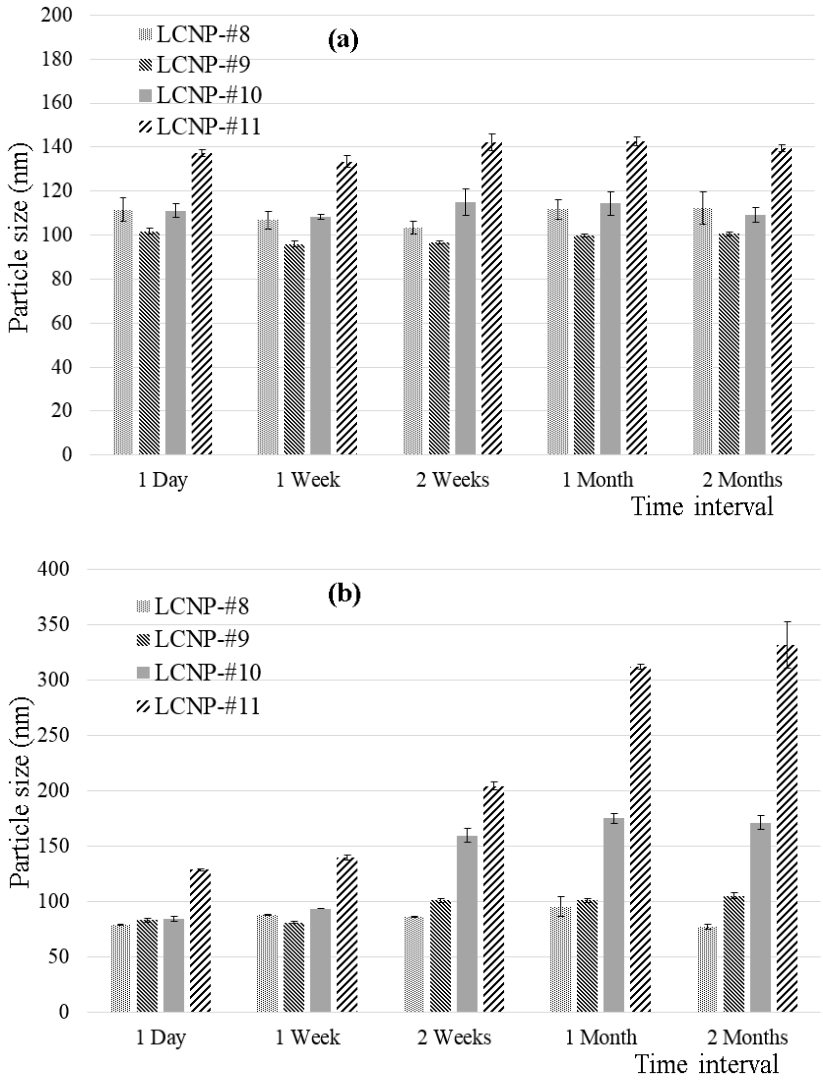

Pharmacokinetic studies

The *in vitro* release patterns of BMK-20113 from the HGC and LCNPs are shown in Figure 12. For the HGC, 3.87% of the BMK-20113 was released

within 3 h, followed by 3.51% in the next 69 h. The evaluation of LCNP-#11 showed that 19.5% of BMK-20113 was released within 12 h, with a 1.65%/h release rate (R^2 = 0.995). This was followed by 32.0% release in the next 60 h, with a 0.518%/h release rate in a sustained manner (R^2 = 0.955).

Figure 12. Cumulative release (0–72 h) of BMK-20113 from the host–guest complex (HGC, control solution) and liquid crystal nanoparticles (LCNP-#11); n = 3.

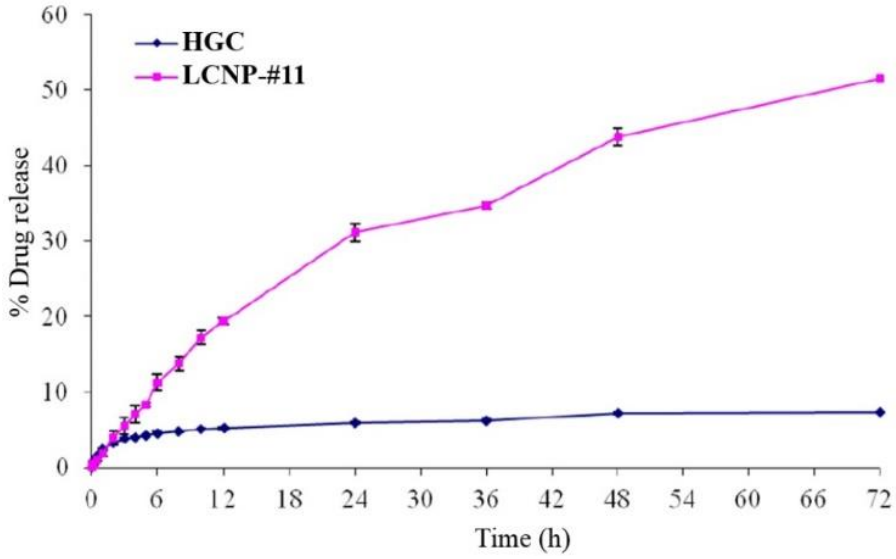

The results of the PK studies following IV and PO administration of HGC and LCNP-#11 in rats are shown in Table 4 and Figure 13. Significant differences were observed between HGC and LCNPs in the maximum concentration (C_{max}), clearance rate (CL_z/F), release pattern, and bioavailability (F) of BMK-20113. With PO administration, the C_{max} value with the LCNPs was twofold higher than that with HGC, and the peptide-

based drug in the LCNPs was released in a sustained manner. In addition, a sudden increase in the drug concentration was observed with the HGC with PO administration. A significant increase (fivefold) in F value was observed with PO administration of LCNPs compared with the HGC.

Table 4. Results of pharmacokinetic studies

		HGC		LCNP-#11	
		IV	PO	IV	PO
$T_{1/2Z}$	h	1.50 ± 0.565	2.23 ± 0.312	1.50 ± 0.847	2.06 ± 0.616
T_{max}	h	-	2.40 ± 0.894	-	1.30 ± 1.52
C_{max}	nmol/L	20,600 ± 4,890	149 ± 40.7	3,340 ± 1420	306 ± 119
$AUC_{(0-t)}$	h·nmol/L	11,200 ± 2,640	686 ± 259	3,030 ± 459	999 ± 220
$AUC_{(0-\infty)}$	h·nmol/L	11,200 ± 2,650	762 ± 270	3,100 ± 495	1,070 ± 202
V_z/F	L/kg	1.43 ± 0.876	3.63 ± 0.678	4.74 ± 2.92	2.72 ± 0.377
CL_z/F	L/h/kg	0.617 ± 157	61.1 ± 21.6	2.16 ± 0.301	38.5 ± 15.0
$MRT_{(0-t)}$	h	0.761 ± 0.0864	18.8 ± 5.67	1.22 ± 0.349	12.7 ± 2.48
F	%	-	3.08 ± 1.16	-	16.5 ± 3.62

Notes: Results of pharmacokinetic studies of the HGC and LCNPs incorporated with BMK-20113.

Abbreviations: HGC, host-guest complex; LCNPs, liquid crystal nanoparticles; IV, intravenous; PO, oral; $T_{1/2Z}$, terminal elimination half-life; C_{max}, maximum concentration; T_{max}, time to C_{max}; CL_z/F, clearance rate; AUC, area under the curve; V_z/F, volume of distribution; $MRT_{(0-t)}$, mean retention time; F, bioavailability.

Figure 13. Plasma concentrations (nmol/L) of BMK-20113 incorporated in host–guest complex (HGC) and liquid crystal nanoparticles (LCNPs)-#11 in male Sprague-Dawley rats after a 10 mg/kg oral (PO) dose, n = 5.

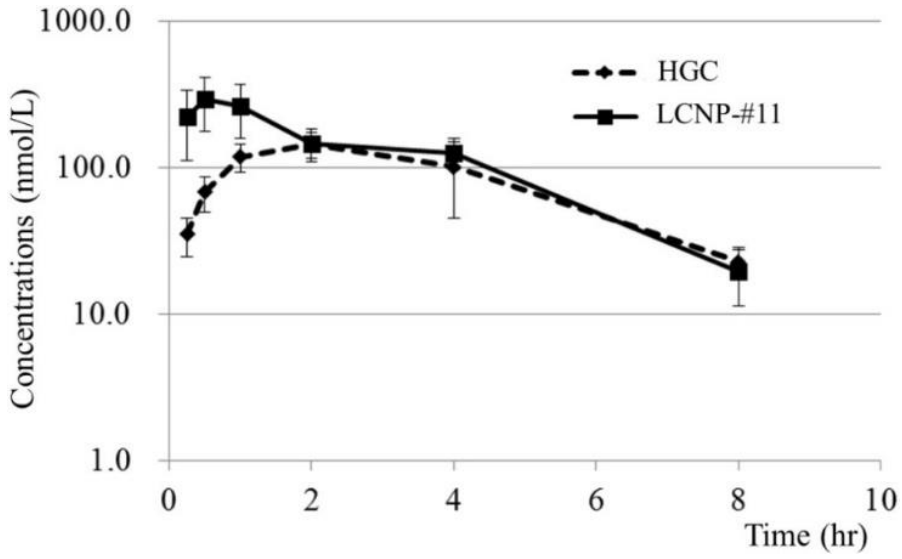

Tissue distribution studies

The tissue distributions of BMK-20113 after IV administrations of the test compound in the HGC and LCNPs are described in Figure 14. The plasma concentration of BMK-20113 after dosing with the LCNP formulation was lower than that resulting from the HGC formulation, in line with the results shown in Table 4, which presumably results from the prolonged retention of LCNPs in the tissues. As shown in Figure 14(a), the concentration of BMK-20113 after dosing with the LCNP formulation is the highest in the liver, while after dosing with the HGC formulation the concentration of BMK-20113 is higher in the kidney, plasma, and lung than in the liver. Furthermore, the liver/plasma distribution ratio in the LCNP formulation is more than 10-fold higher than that in the HGC formulation, as shown in Figure 14(b).

Regarding the distribution to the kidney and lung, the ratios in the LCNP formulation are higher than those in the HGC formulation; however, the drug concentrations in the LCNP formulation are lower than those in the HGC formulation. This shows that BMK-20113 in the LCNP formulation is specifically distributed into the liver, while that in the HGC formulation is distributed into the plasma, kidney, liver, and lung nonspecifically. Additionally, the concentration in CSF is very low with the LCNP formulation, less than one-seventh of that observed with the HGC formulation, which indicates that the LCNP formulation does not allow noticeable blood–brain barrier penetration.

Figure 14. Concentrations and tissue distributions of BMK-20113 incorporated into host–guest complex (HGC) and liquid crystal nanoparticles (LCNP)-#11. (a) Concentrations of BMK-20113 in tissues, in male Sprague-Dawley rats 5 min after a 5 mg/kg intravenous (IV) dose of BMK-20113 incorporated into HGC or LCNP-#11, n = 3. (b) Ratio of the concentration of BMK-20113 in tissue to that in plasma after oral dose of BMK-20113 incorporated into HGC or LCNP-#11. CSF, cerebrospinal fluid.

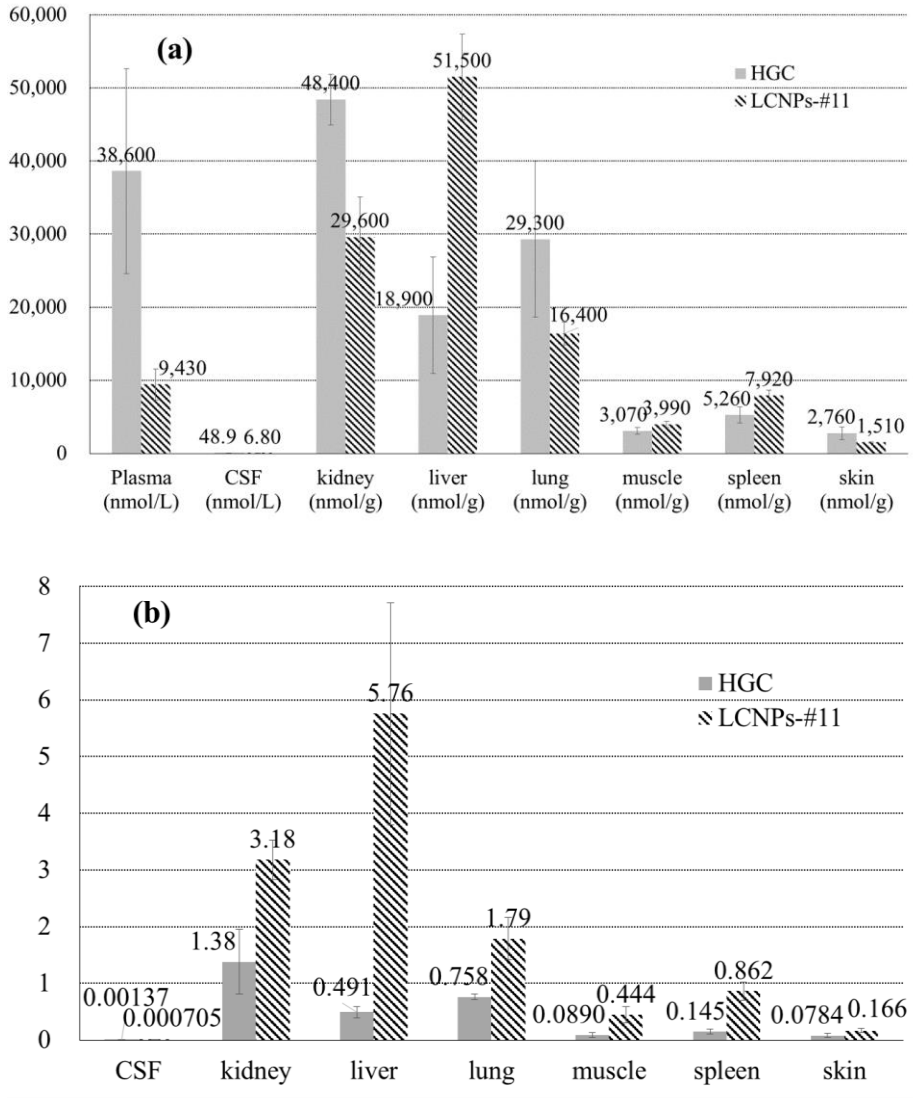

III. Discussion

The LCNPs in this study were prepared by simple heating of the complex to 85℃, followed by rapid cooling to 25℃ in a minute. Therefore, the energy input required for the preparation was much lower than that required for high-pressure homogenization and ultrasonication, which are used in the conventional preparation. Therefore, the industrial preparation of LCNPs using the method in this study could be more convenient than that with conventional methods. As illustrated in Figure 2, the conductivity was around 140 μS at 80°C and with a temperature increase to 95°C, it fell below 20 μS. During the conductivity change period, the appearance of the complex changed from turbid to semi-transparent. This change in appearance signified that the complex phase had changed from the melt-lipid in water emulsion to a bicontinuous phase.[24] The solubility of BMK-20113 in the lipid phase was improved as the temperature increased. Therefore, the dissolution process for BMK-20113 was endothermic, and recrystallization or aggregation of BMK-20113 could occur at low temperatures. At 4℃, there was no aggregation and recrystallization of the poorly water-soluble BMK-20113;[22] therefore, it can be concluded that BMK-20113 was encapsulated in the liquid crystal structure of the LCNPs. One major concern with the heating process during the preparation of lipid nanocapsules is the degradation of the drug during the process. There was no change in the HPLC analysis of BMK-20113 during the preparation of the LCNPs compared to the original BMK-20113 in tetrahydrofuran, which confirmed the stability of BMK-20113 under the heating conditions, as shown in Figure 3.

The SAXD analysis revealed that the surface of the LCNPs is composed of a lipid lamellar phase with a periodicity of 9.7 nm. In the WAXD analysis, the alkyl chains of octadecanol, hexadecanol, and the surfactants are positioned at distances of 0.419 and 0.379 nm, respectively, which means that the LCNPs

are composed of orthorhombic lateral packing, as illustrated in Figure 5. The lamellar liquid structure is considered suitable for drug delivery because the sustained drug release was reported to be possible with the multilayer structured carrier.[25] There was no difference in the SAXD and WAXD patterns with increasing concentrations of BMK-20113. Therefore, it can be concluded that the lateral packing of lipids at the surface of the LCNPs was not concentration-dependent. It can also be predicted that the controlled release of the drug was possible because of the layer-by-layer erosion of the drug from the lamellar liquid crystal structure.[25b]

The DSC evaluation of the LCNPs showed a main peak at 35℃, which is lower than the melting peaks of excipients (Figure 6 and Figure 7). As reported by Montenegro *et al,*[26] the melting peak of cetyl palmitate could be lower than the peak of the cetyl palmitate bulk. This lower melting point could be attributed to the nano size of the particles and the non-crystallized, super-cooled state of the core of the LCNPs.[26-27] The state of tetradecyl tetradecanoate in the LCNP layer in this study was nano-sized and could also be the super-cooled form resulting from the rapid cooling process. This phenomenon may explain the decrease in the melting point.

Because the melting peak of the LCNPs is observed at 34-36℃, the particle could melt after oral dosing and the coalescence of the particles could follow. Because the coalescence results in destabilization of the formulation, it is not suitable for oral administration. In order to ensure the stability under the PK evaluation conditions, the stability of the LCNPs was evaluated using dynamic light scattering at 4 and 37℃, as shown in Figure 11. It should be noted that the stability at 37℃ was important to ensure the stability of the vehicle under the conditions of the PK study. At 4℃, there was no significant change in particle size for 2 months, which means that the LCNPs are stable under that condition. However, an increase was observed in the particle size

when the LCNPs were stored at 37℃. The particle size of the LCNPs was preserved for up to 1 week; however, it significantly increased 2 weeks after the incorporation of 1.50 and 2.50 wt% BMK-20113 to the lipid mix (LCNP-#10 and #11, respectively). It can be assumed that the addition of BMK-20113 to the LCNPs at a concentration higher than 1.50 wt% (LCNP-#10) affects the amorphous property of the core, which presumably leads to the acceleration of coalescence and Ostwald ripening. Furthermore, the lipids in the LCNPs are converted to liquid form above 35℃, as shown by the DSC results. Therefore, the coalescence and Ostwald ripening could be stimulated at 37℃, thereby increasing the particle size and destabilizing the LCNPs. However, the stability of the LCNPs at 37℃ is acceptable for the PK study since the test is performed within 2 to 3 days. The acceptable stability of the LCNPs at 37℃ can be rationalized based upon the retardation of coalescence because of the repulsive forces produced by the PEG group of PEG-12 cetostearyl ether.[28] Because of the repulsive forces, the surface layer comprising the surfactant can act as a physical barrier, therefore the formulation can be stable for 1 week. As for the stability in the acidic condition, the particle shapes and sizes of LCNP-#8 and #11 were comparable with those in the neutral condition. Therefore, it can be assumed that the LCNPs are durable under the stomach environment.

As shown in Figure 12, sustained release of BMK-20113 incorporated in the LCNPs was observed until 72 h, compared with the HGC formulation, which showed a very low drug release rate. Because the evaluation was carried out below the saturation point of BMK-20113, it clearly indicates that the sustained release is possible with the LCNPs. The results can be explained by the structure of the LCNPs, as determined by SAXD and WAXD. These analyses showed that the drug release can be controlled by the layer-by-layer erosion of the orthorhombic lateral packing structure of the LCNPs at 37℃.[25b]

Conversely, the HGC is composed of 2-hydroxypropyl-β-cyclodextrin (HP-β-CD) as the host incorporated with the peptide-based therapeutic BMK-20113, which is the guest with a cyclic structure. The structure is efficient for incorporating the hydrophobic drug with the hydrophobic site of HP-β-CD; however, the drug release can be delayed or inhibited if the affinity of the bond between the HP-β-CD and the peptide-based is too strong.[29] Additionally, the loading efficiency of the BMK-20113 was 25.0 mg in 1.00 g of the LCNPs, which is much higher compared with that for the HGC at 5.88 mg in 1.00 g of the complex. The enhanced efficiency of the drug loading can be explained by the amorphous state of the LCNP core. This complex core is composed of tetradecyl tetradecanoate, cetyl palmitate, glyceryl stearate, hexadecanol, and octadecanol, which provides more room for the encapsulation of BMK-20113.[30]

In the PK study shown in Table 4, the bioavailability of the BMK-20113 incorporated in the LCNPs is more than five times higher than that with the HGC. In addition, the $T_{1/2Z}$ of the LCNP–BMK-20113 complex was comparable with that of the HGC–BMK-20113 complex. The mean retention time (MRT) of the PO dosing was higher for the HGC compared to the LCNP, as shown by the sudden increase in drug concentration observed at 1, 2, and 4 hours in the HGC (Figure 13). Therefore, the half-life and MRT could have been retarded during the evaluation of the HGC. The amounts of BMK-20113 released from the HGC at 1, 2, and 4 hours were about twice as high as that at 0.25 h. Conversely, sustained release of BMK-20113 was observed from the LCNPs and the concentration was maintained at a constant level from 0.25 to 4 h, which suggests that the drug release was uniform. With these results, it can be concluded that drug delivery with the LCNPs is more efficient than that with the HGC. These results are in agreement with the predicted properties obtained from the dialysis, SAXD, and WAXD analysis. The

improvement in the bioavailability of the BMK-20113 incorporated in the LCNPs is presumably attributable to the multi-layer structure of LCNPs, which offers sustained drug release.[25a] In addition, the liquid crystal structure protects the drug within the gastrointestinal tract, thereby enhancing its stability because the drug is encapsulated in the lipid core. Moreover, the outer layer is PEGylated with ceteareth-12 and ceteareth-20, which function as a stealth layer under gastrointestinal conditions; therefore, the BMK-20113 incorporated into the LCNPs is more stable than that with the HGC.[18, 31]

From the tissue distribution study, it can be reasoned that the hydrophobic peptide-based drug is delivered specifically to the liver when it is incorporated into the LCNPs. As described in the results, the distribution into the liver with LCNP-#11 is more than 10-fold higher than that with HGC. The concentrations in the kidney and lung from the LCNP formulation are higher than those from the HGC formulation. However, the higher values are not because of selective delivery to the kidney and lung by the LCNPs but because of the lower plasma concentration with the LCNP formulation compared to that with the HGC formulation, as shown in Figure 14(a). Therefore, it can be concluded that the LCNPs are a more liver-specific drug delivery system than the HGC. The liver-specific drug delivery can be rationalized with the mechanism of lipid metabolism.[21] In the reported mechanism, the emulsions can be metabolized via the comparable metabolism pathway of chylomicron or removed from the plasma by the cells of the mononuclear phagocyte system when the emulsions are recognized as foreign materials.[21a] If the LCNPs are recognized as a foreign material, then the concentration of BMK-20113 should be significantly reduced in the blood within 30 min or less and should be increased in both the liver and spleen because of the mononuclear phagocyte system, the Kupffer cells of the liver, and the macrophages of the spleen.[21a] However, the concentrations are

preserved at a certain level until 1 hour after IV and 4 hour after PO administration, as shown in Table 4 and Figure 13. Another plausible mechanism for liver-specific delivery is that the LCNPs can be metabolized via the lipid emulsion metabolism pathway. As it was reported in the drug delivery system with lipid emulsions, the emulsion can be recognized as artificial chylomicrons.[32] Because the LCNPs melt at the body temperature, it also can be recognized as artificial chylomicrons which enable the specific accumulation into liver. Furthermore, in the body distribution study, the concentration in the spleen with the LCNP formulation is not significantly different from that with the HGC formulation while the difference in the liver is significant, as shown in Figure 14(a). From the results, it can be seen that the LCNPs are specifically delivered to the liver by avoiding clearance by the mononuclear phagocyte system, presumably because of the PEG groups of the surfactants and the reduced particle size.

IV. Conclusion

In this study, the LCNPs incorporated with the peptide-based therapeutic were prepared using the PIT method, which required low energy input with a short processing time. The structure of the LCNPs was determined to be orthorhombic lateral packing with a lamellar liquid crystal structure, and the particle sizes was around 100 nm. The stability of the LCNPs was confirmed with the particle size analysis at 4℃. The BMK-20113 incorporated in the LCNPs was stable during the PIT procedure and the loading efficiency of the LCNPs was 2.5 wt% for the lipid mix and 0.75 wt% for the dispersion, which was higher than that for the HGC. The dialysis test confirmed the sustained release of the drug incorporated in the LCNPs. The PK study showed that the F value of the LCNP–BMK-20113 complex increased fivefold compared with that for the HGC–BMK-20113 complex. The improvement in the F value and sustained release are in agreement with the predicted properties of the liquid crystal structure of the LCNPs. The liquid crystal structure facilitated the controlled release of the drug and the F value was improved because the LCNPs were stable under the gastrointestinal conditions owing to the PEGylated surface, which acts as a stealth layer. Furthermore, it was revealed in the tissue distribution study that the LCNPs are a liver-specific drug delivery system.

V. Experimental

Materials

BMK-20113 was synthesized in our lab and its structure and activity were described in our previous report.[22] Emulgade® SE-PF, tetradecyl tetradecanoate (Cetiol® MM, myristyl myristate), PEG-15 hydroxystearate (Solutol® HS 15), and PEG-12 cetostearyl ether (Eumulgin® B 1, ceteareth-12) were kindly provided by BASF SE (Dusseldorf, Germany). HP-β-CD was purchased from Aldrich (St. Louis, Missouri, USA). Carbopol 980 NF was purchased from Shanghai Chineway Pharmaceutical Technology (Shanghai, China). The water used in the sample preparation, HPLC, and liquid chromatography-mass spectrometry (LC-MS/MS) procedures and the isopropyl alcohol used in the HPLC procedure were of HPLC grade and were purchased from Fisher Scientific (Hampton, New Hampshire, USA). All other reagents were of analytical grade and were used as supplied.

Preparation of LCNPs and HGC

The compositions of the LCNP formulations are described in Table 1 and the PIT method used for preparing the formulations is as follows: First, the lipid (composed of lipids, drug, and surfactants) and aqueous portions were heated separately at about 85℃. The aqueous portion was then added to the lipid portion and stirred until the hazy mixture turned semi-transparent. The mixture was then cooled to 25℃ in a water bath containing ice for 1 min to obtain the LCNPs. The PIT was measured with a conductivity meter (Cond 6+, Eutech Instrument, Singapore), which measures the conductivity change at the emulsion inversion zone.

LCNP formulations with the compositions described in Table 2 were prepared for the PK and structure analysis. The procedure for the preparation of these formulations was the same as that described above for the LCNPs. For the HGCs, 20.0 g of HP-β-CD was slowly added to 100 mL of purified water to form a solution, which was vortexed until clear. Then 0.5 mL of PEG-15 hydroxystearate was added to 0.25 mL of dimethyl sulfoxide (DMSO) incorporated with 5.00 mg of BMK-20113, and this solution was mixed until clear. The BMK-20113 solution was added to 4.25 mL of the HP-β-CD solution and then vortexed until clear. The prepared LCNPs and HGC were stored at 4℃ for further evaluation.

SAXD and WAXD analysis

The structures of the LCNPs were characterized using SAXD and WAXD analyses carried out on a SAXSpace (Anton-Paar, Graz, Austria) at the National Instrumentation Center for Environmental Management (NICEM, Seoul, Korea). The scattering intensity was estimated as a function of the scattering vector q which is defined as $q = (4\pi\sin\theta)/\lambda$, where θ and λ stand for the scattering angle and wavelength, respectively. The distances between the planes of the LCNP surface (d) were calculated from the obtained indexing peaks in the SAXD scattering patterns using Bragg's equation, $d = 2\pi/q$. The calculated inter-planar distances were multiplied by the peak ratio of the particular peak. The packing structure of the LCNPs was determined using WAXD. The scattering patterns were compared with the patterns previously reported by Bouwstra *et al.*[23]

TEM analysis

A 0.10 mL aliquot of the LCNP dispersion was diluted in 1.0 mL of water or hydrochloric acid-potassium chloride buffer (HCl-KCl) solution (0.2 M, pH 1.5) at 25℃. The diluted dispersion was dropped on to CF300-Cu carbon film (Electron Microscopy Sciences, Hatfield PA, USA) and then dried for 1 day under reduced pressure. The TEM images were obtained on JEOL EM-2010 and JEM-3010 microscopes (JEOL, Tokyo, Japan) at an accelerating voltage of 200 kV.

Particle size analysis

The particle size was evaluated using dynamic light scattering, which yields the mean particle size and particle size distribution. Approximately 0.2 mL of the LCNP dispersion was diluted in 10 mL of purified water at 25℃. Then 3 mL of the diluted dispersion was added to a φ21 cylinder cell in a particle size analyzer (DLS-8000HL, Otsuka Electronics, Osaka, Japan), which was equipped with a 10-mW He-Ne Laser. The evaluation was performed 30 times for each dispersion at a detection angle of 90° and the measurement was repeated three times.

In vitro dialysis

To avoid the potential precipitation of BMK-20113 a modified assay was used, as previously reported by Hua.[33] To prepare the donor solution, 1.5 mL of the HGC dispersion was mixed with 4 mL of 0.5 wt% carbopol gel and then dispersed into 38.5 mL of the dissolution medium, which was 50 mM phosphate-buffered saline (PBS, pH 6.5). To prepare the LCNP dispersion donor solution, 0.2 mL of LCNP-#11 was mixed with 4 mL of 0.5 wt% carbopol gel and then dispersed into 39.8 mL of the dissolution medium. A

total of 11 mL of the donor solution was added to a dialysis bag (10 kDa molecular weight cut off, Thermo Fisher Scientific, Waltham, MA USA) and this was suspended in 90 mL of the acceptor solution, which was the dissolution medium. At scheduled intervals, 400 µL of the acceptor solution was collected for HPLC assay and an equal volume of fresh dissolution medium was added to maintain a constant volume. The concentration of BMK-20113 in the collected sample was determined by HPLC.

Pharmacokinetic studies

The Sprague-Dawley rats (184–238 g body weight) used in the study were supplied by Sipper-BK Lab Animal Ltd (Shanghai, China). For the intravenous (IV) and oral (PO) dose group, the nominal concentration of the dosing solutions was 1.0 mg/mL. The study was designed as described in Table 3 and conducted in parallel with the two formulations (HGC and LCNP-#11) as described in Table 2. Individual doses were calculated based on pre-treatment body weights recorded on the day of dose administration. The IV dose was administered via the tail vein as a bolus injection, and each animal received 5 mL of the solution per kg of body weight. For the PO dose, each animal was administered 10 mL of the solution per kg of body weight via a gavage tube. Blood (0.2–0.3 mL) was collected in polypropylene tubes containing ethylenediaminetetraacetic acid (EDTA)-K_2 as an anticoagulant, at different time points and then stored on wet ice until processed for plasma by centrifugation. The samples were centrifuged at 6000 rpm for 8 min within 1 h of blood collection. The plasma samples were then stored at approximately -20℃ until analyzed by LC-MS/MS with an internal standard. The lower limit of quantification of BMK-20113 was 1.0 nmol/L. Pharmacokinetic parameters

were calculated with WinNonlin® 6.3 through the use of Non-compartmental pharmacokinetic analysis method.

Tissue distribution studies

Six Sprague-Dawley rats (190–216 g in body weight) supplied by Sippr-BK Lab Animal Ltd. (Shanghai, China) were used in this study. The nominal concentration of the dose solution was 1.0 mg/mL. For the study, six male Sprague-Dawley rats were divided into two groups; the animals in group 1 and group 2 were given a single IV dose with HGC and LCNP-#11, respectively, at a nominal dose of 5 mg/kg as a 1 mg/mL solution. Individual doses were calculated based on pre-dose body weights recorded on the day of dose administration. For IV dose, administered via tail vein as a bolus injection, which are presented in Table 5. Samples of the cerebrospinal fluid (CSF), blood (0.150–0.200 mL), lung, liver, kidney, spleen, skin, and muscle were collected into polypropylene tubes containing EDTA-K2 as the anticoagulant and stored on wet ice until processed for plasma by centrifugation. The samples were centrifuged within 30 minutes of blood collection at 6000 rpm for 8 minutes and the plasma samples were then stored in a freezer until analyzed by LC-MS/MS. The tissues were homogenized with five volumes of PBS to obtain a tissue suspension.

Table 5. Body weights and dose volumes of Sprague-Dawley rats for the tissue distribution study

Group	Animal ID	Body weight (g)	Dose route	Dose volume (mL)
1	101#	212	IV	1.06
1	102#	190	IV	0.95
1	103#	210	IV	1.05
2	201#	210	IV	1.05
2	202#	200	IV	1.00
2	203#	216	IV	1.08

LC-MS/MS analysis in the body distribution study

LC-MS/MS analysis of plasma, kidney, liver, skin, and spleen samples was carried out using a Shimadzu LC-20AD coupled with an AB Sciex API 4000 (Shimadzu, Kyoto, Japan). Standard curve samples (20 µL), QC samples and rat plasma samples were mixed with 60 µL of acetonitrile containing internal standard (200 ng/mL of tolbutamide or 50 ng/mL of propranolol) in EP tubes. After vortexing the mixture for 1 min, the mixture was centrifuged for 10 min at 13,000 rpm at 4 ℃ and then the supernatant (50 µL) was transferred to a 96-well plate which was pre-added in 150 µL of water. After shaking the samples for 10 min, 10 µL of sample was injected into LC-MS/MS. The separation was carried out on a Thermo Betasil C18 column (2.1 × 50 mm, 5-µm particle size) with 0.1% TFA in water (A) and acetonitrile (B) as the mobile phase at a flow rate of 0.5 mL/min. Method: 10% B (0–0.5 min), 10–95% B (0.5–1.1 min), 95% B (1.1–1.4 min), 95–10% B (1.4–1.5 min), 10% B (1.5–2.2 min). Mass transitions: 260.3/116.2 for propranolol (internal standard); 761.4/289.1 for BMK-20113.

The lung, muscle, and CSF samples were analyzed by LC-MS/MS using a Shimadzu LC-20AD coupled with an AB Sciex API 4000. The other analytical conditions are the same as those used for the plasma, kidney, liver, skin, and spleen samples.

Reference

Part I.

1. Barry, B. W. *Adv. Drug Deliver. Rev.* **2002,** *54*, S31-S40.

2. Bouwstra, J. A.; Gooris, G. S.; Vanderspek, J. A.; Bras, W. *J. Invest. Dermatol.* **1991,** *97* (6), 1005-1012.

3. Lapteva, M.; Kalia, Y. N. *Expert Opin. Drug Del.* **2013,** *10* (8), 1043-1059.

4. Kanikkannan, N.; Singh, M. *Int. J. Pharm.* **2002,** *248* (1-2), 219-228.

5. Narang, A. S.; Delmarre, D.; Gao, D. *Int. J. Pharm.* **2007,** *345* (1-2), 9-25.

6. Martins, S.; Sarmento, B.; Ferreira, D. C.; Souto, E. B. *Int. J. Nanomed.* **2007,** *2* (4), 595-607.

7. (a) Yoon, G.; Park, J. W.; Yoon, I.-S. *J. Pharm. Investig.* **2013,** *43* (5), 353-362; (b) Natarajan, J. V.; Nugraha, C.; Ng, X. W.; Venkatraman, S. *J. Control. Release* **2014,** *193*, 122-138; (c) Weber, S.; Zimmer, A.; Pardeike, J. *Eur. J. Pharm. Biopharm.* **2014,** *86* (1), 7-22.

8. (a) Elsayed, M. M. A.; Abdallah, O. Y.; Naggar, V. F.; Khalafallah, N. M. *Int. J. Pharm.* **2007,** *332* (1-2), 1-16; (b) Feld, J.; Barta, S. K.; Schinke, C.; Braunschweig, I.; Zhou, Y. Y.; Verma, A. K. *Oncotarget* **2013,** *4* (3), 397-412.

9. (a) Friberg, S. *J. Colloid. Interf. Sci.* **1971,** *37* (2), 291-&; (b) Nesseem, D. I. *J. Pharmaceut. Biomed.* **2001,** *26* (3), 387-399; (c) Muller-Goymann, C. C. *Eur. J. Pharm. Biopharm.* **2004,** *58* (2), 343-356; (d) Otto, A.; du Plessis, J.; Wiechers, J. W. *Int. J. Cosmet. Sci.* **2009,** *31* (1), 1-19; (e) Hosmer, J. M.; Steiner, A. A.; Lopes, L. B. *Pharm. Res.* **2013,** *30* (3), 694-706.

10. Fong, W. K.; Hanley, T.; Boyd, B. J. *J. Control. Release* **2009,** *135* (3), 218-226.

11. Al-Bawab, A.; Friberg, S. E. *Adv. Colloid Interface Sci.* **2006,** *123*, 313-

322.

12. Zhang, W.; Liu, L. *J. Cosmet. Dermatol. Sci. Appl.* **2013,** *03* (02), 139-144.

13. (a) Lucek, R. W.; Colburn, W. A. *Clin. Pharmacokinet.* **1985,** *10* (1), 38-62; (b) Melot, M.; Pudney, P. D. A.; Williamson, A. M.; Caspers, P. J.; Van Der Pol, A.; Puppels, G. J. *J. Control. Release* **2009,** *138* (1), 32-39; (c) Lee, S. J.; Cho, S. A.; An, S. S.; Na, Y. J.; Park, N. H.; Kim, H. S.; Lee, C. W.; Kim, H. K.; Kim, E. K.; Jang, Y. P.; Kim, J. W. *Evid-Based Compl. Alt.* **2012**.

14. Ries, G.; Hess, R. *J. Toxicol-Cutan. Ocul.* **1999,** *18* (3), 169-185.

15. (a) Chorilli, M.; Prestes, P. S.; Rigon, R. B.; Leonardi, G. R.; Chiavacci, L. A.; Sarmento, V. H. V.; Oliveira, A. G.; Scarpa, M. V. *Colloid Surface B* **2011,** *85* (2), 182-188; (b) Oliveira, M. B.; do Prado, A. H.; Bernegossi, J.; Sato, C. S.; Brunetti, I. L.; Scarpa, M. V.; Leonardi, G. R.; Friberg, S. E.; Chorilli, M. *Biomed. Res. Int.* **2014**; (c) Sub, D. C.; Kim, Y.; Kim, H.; Ro, J.; Cho, S. W.; Yun, G.; Choi, S. U.; Lee, J. *Biomol. Ther.* **2014,** *22* (1), 73-77.

16. (a) Alam, M. M.; Aramaki, K. *J. Colloid Interf. Sci.* **2009,** *336* (1), 329-334; (b) Mao, L.; Calligaris, S.; Barba, L.; Miao, S. *Food Res. Int.* **2014,** *58*, 81-88.

17. Dong, Y. D.; Boyd, B. J. *Int. J. Pharm.* **2011,** *417* (1-2), 101-111.

18. Bueno, J. M. *J. Opt. A-Pure Appl. Op.* **2000,** *2* (3), 216-222.

19. (a) Dillet, J.; Baravian, C.; Caton, F.; Parker, A. *Appl. Optics* **2006,** *45* (19), 4669-4678; (b) Arteaga, O.; Baldris, M.; Anto, J.; Canillas, A.; Pascual, E.; Bertran, E. *Appl. Optics* **2014,** *53* (10), 2236-2245.

20. Caspers, P. J.; Lucassen, G. W.; Carter, E. A.; Bruining, H. A.; Puppels, G. J. *J. Invest. Dermatol.* **2001,** *116* (3), 434-442.

21. Pudney, P. D. A.; Melot, M.; Caspers, P. J.; van der Pol, A.; Puppels, G. J. *Appl. Spectrosc.* **2007,** *61* (8), 804-811.

22. Smith, G. P. S.; McGoverin, C. M.; Fraser, S. J.; Gordon, K. C. *Adv. Drug*

Deliver. Rev. **2015,** *89*, 21-41.

23. Bouwstra, J. A.; Gooris, G. S.; Dubbelaar, F. E. R.; Ponec, M. *J. Invest. Dermatol.* **2002,** *118* (4), 606-617.

24. Kitzerow, H. S. *Liq. Cryst.* **1994,** *16* (1), 1-31.

25. (a) Pezzaniti, J. L.; Chipman, R. A. *Opt. Eng.* **1995,** *34* (6), 1558-1568; (b) Chipman, R. A.; Bass, M. *Handbook of Optics. Polarimetry*, 2nd ed.; McGraw Hill: New York, 1995.

26. Friberg, S. E. *J. Soc. Cosmet. Chem.* **1990,** *41* (3), 155-171.

27. Vucinic-Milankovic, N.; Savic, S.; Vuleta, G.; Vucinic, S. *Drug Dev. Ind. Pharm.* **2007,** *33* (3), 221-234.

28. Horvath-Szabo, G.; Masliyah, J. H.; Czarnecki, J. *J. Colloid Interf. Sci.* **2003,** *257* (2), 299-309.

29. Hosmer, J. M.; Steiner, A. A.; Lopes, L. B. *Pharm. Res-Dordr.* **2013,** *30* (3), 694-706.

30. (a) Iwai, H.; Fukasawa, J.; Suzuki, T. *Int. J. Cosmet. Sci.* **1998,** *20* (2), 87-102; (b) Holler, S.; Valenta, C. *Eur. J. Pharm. Biopharm.* **2007,** *66* (1), 120-6.

31. Eccleston, G. M. *J. Soc. Cosmet. Chem.* **1990,** *41* (1), 1-22.

32. Everall, N. J. *Appl. Spectrosc.* **2000,** *54* (10), 1515-1520.

33. (a) Wascotte, V.; Caspers, P.; de Sterke, J.; Jadoul, M.; Guy, R. H.; Preat, V. *Pharm. Res-Dordr.* **2007,** *24* (10), 1897-1901; (b) Mateus, R.; Abdalghafor, H.; Oliveira, G.; Hadgraft, J.; Lane, M. E. *Int. J. Pharm.* **2013,** *444* (1-2), 106-108.

Part II.

1. (a) Craik, D. J.; Fairlie, D. P.; Liras, S.; Price, D. *Chem. Biol. Drug Des.* **2013,** *81* (1), 136-147; (b) Kaspar, A. A.; Reichert, J. M. *Drug Discov. Today* **2013,** *18* (17-18), 807-817.

2. (a) Leader, B.; Baca, Q. J.; Golan, D. E. *Nat. Rev. Drug Discov.* **2008,** *7* (1), 21-39; (b) Vlieghe, P.; Lisowski, V.; Martinez, J.; Khrestchatisky, M. *Drug Discov. Today* **2010,** *15* (1-2), 40-56; (c) Collins, I.; Workman, P. *Nat. Chem. Biol.* **2006,** *2* (12), 689-700.

3. Tice, C. M.; Singh, S. B. Evolution of Diverse Classes of Renin Inhibitors Through the Years. In *Aspartic Acid Proteases as Therapeutic Targets*; Ghosh, A. K., Ed.; Wiley-VCH: Weinheim, Germany, 2010; pp 297-324.

4. (a) Torchilin, V. P. *Nat. Rev. Drug Discov.* **2005,** *4* (2), 145-160; (b) Martins, S.; Sarmento, B.; Ferreira, D. C.; Souto, E. B. *Int. J. Nanomed.* **2007,** *2* (4), 595-607; (c) Mohanraj, V. J.; Barnes, T. J.; Prestidge, C. A. *Int. J. Pharmaceut.* **2010,** *392* (1-2), 285-293; (d) Niu, M. M.; Lu, Y.; Hovgaard, L.; Wu, W. *Int. J. Nanomed.* **2011,** *6*, 1155-1166.

5. (a) Veronese, F. M.; Pasut, G. *Drug Discov. Today* **2005,** *10* (21), 1451-1458; (b) Roberts, M. J.; Bentley, M. D.; Harris, J. M. *Adv. Drug Deliver. Rev.* **2012,** *64*, 116-127.

6. (a) Hirsjarvi, S.; Belloche, C.; Hindre, F.; Garcion, E.; Benoit, J. P. *Eur. J. Pharm. Biopharm.* **2014,** *87* (1), 152-159; (b) Watnasirichaikul, S.; Davies, N. M.; Rades, T.; Tucker, I. G. *Pharmaceut. Res.* **2000,** *17* (6), 684-689.

7. Almeida, A. J.; Runge, S.; Muller, R. H. *Int. J. Pharmaceut.* **1997,** *149* (2), 255-265.

8. Zeng, N.; Gao, X. L.; Hu, Q. Y.; Song, Q. X.; Xia, H. M.; Liu, Z. Y.; Gu, G. Z.; Jiang, M. Y.; Pang, Z. Q.; Chen, H. Z.; Chen, J.; Fang, L. *Int. J. Nanomed.*

2012, *7*, 3703-3718.

9. Kumar, M.; Gupta, D.; Singh, G.; Sharma, S.; Bhat, M.; Prashant, C. K.; Dinda, A. K.; Kharbanda, S.; Kufe, D.; Singh, H. *Cancer Res.* **2014,** *74* (12), 3271-3281.

10. (a) Huynh, N. T.; Passirani, C.; Saulnier, P.; Benoit, J. P. *Int. J. Pharmaceut.* **2009,** *379* (2), 201-209; (b) Park, K.; Kwon, I. C.; Park, K. *React. Funct. Polym.* **2011,** *71* (3), 280-287.

11. (a) Tangso, K. J.; Lindberg, S.; Hartley, P. G.; Knott, R.; Spicer, P.; Boyd, B. J. *ACS Appl. Mater. Inter.* **2014,** *6* (15), 12363-12371; (b) Chen, Y. L.; Ma, P. Y.; Gui, S. *Biomed. Res. Int.* **2014**; (c) Murgia, S.; Falchi, A. M.; Mano, M.; Lampis, S.; Angius, R.; Carnerup, A. M.; Schmidt, J.; Diaz, G.; Giacca, M.; Talmon, Y.; Monduzzi, M. *J. Phys. Chem. B* **2010,** *114* (10), 3518-3525; (d) Spillmann, C. M.; Naciri, J.; Algar, W. R.; Medintz, I. L.; Delehanty, J. B. *ACS Nano* **2014,** *8* (7), 6986-6997.

12. (a) Swarnakar, N. K.; Thanki, K.; Jain, S. *Mol. Pharmaceut.* **2014,** *11* (5), 1435-1449; (b) Swarnakar, N. K.; Thanki, K.; Jain, S. *Pharmaceut. Res.* **2014,** *31* (5), 1219-1238.

13. Misra, R.; Mohanty, S. *J. Mater. Sci. Mater. Med.* **2014,** *25* (9), 2095-2109.

14. Mei, Z. N.; Lia, X. K.; Wu, Q. R.; Yang, X. L. *Pharmacol. Res.* **2005,** *51* (4), 345-351.

15. Madheswaran, T.; Baskaran, R.; Thapa, R. K.; Rhyu, J. Y.; Choi, H. Y.; Kim, J. O.; Yong, C. S.; Yoo, B. K. *AAPS Pharmscitech.* **2013,** *14* (1), 45-52.

16. (a) Heurtault, B.; Saulnier, P.; Pech, B.; Proust, J. E.; Benoit, J. P. *Pharmaceut. Res.* **2002,** *19* (6), 875-880; (b) Izquierdo, P.; Esquena, J.; Tadros, T. F.; Dederen, C.; Garcia, M. J.; Azemar, N.; Solans, C. *Langmuir* **2002,** *18* (1), 26-30; (c) Anton, N.; Benoit, J. P.; Saulnier, P. *J. Control. Release* **2008,** *128* (3), 185-199.

17. (a) Zhou, H. F.; Yue, Y.; Liu, G. L.; Li, Y.; Zhang, J.; Yan, Z. M.; Duan, M. X. *Nanoscale Res. Lett.* **2010,** *5* (10), 1561-1569; (b) Peltier, S.; Oger, J. M.; Lagarce, F.; Couet, W.; Benoit, J. P. *Pharmaceut. Res.* **2006,** *23* (6), 1243-1250; (c) Hureaux, J.; Lagarce, F.; Gagnadoux, F.; Vecellio, L.; Clavreul, A.; Roger, E.; Kempf, M.; Racineux, J. L.; Diot, P.; Benoit, J. P.; Urban, T. *Eur. J. Pharm. Biopharm.* **2009,** *73* (2), 239-246.

18. Song, H. F.; Zhang, J.; Han, Z. K.; Zhang, X. Y.; Li, Z.; Zhang, L. Y.; Fu, M.; Lin, C.; Ma, J. *Cancer Chemoth. Pharm.* **2006,** *57* (5), 591-598.

19. Yoon, G.; Park, J. W.; Yoon, I.-S. *J. Pharm. Investig.* **2013,** *43* (5), 353-362.

20. Tongcher, O.; Sigel, R.; Landfester, K. *Langmuir* **2006,** *22* (10), 4504-4511.

21. (a) Rossi, J.; Leroux, J.-C. Principles in the Development of Intravenous Lipid Emulsions. In *Role of Lipid Excipients in Modifying Oral and Parenteral Drug Delivery*; Wasan, K. M. Ed.; Wiley-Interscience: Hoboken, New Jersey, 2006; pp 88-123.; (b) Rensen, P. C. N.; Herijgers, N.; Netscher, M. H.; Meskers, S. C. J.; vanEck, M.; vanBerkel, T. J. C. *J. Lipid Res.* **1997,** *38* (6), 1070-1084.

22. Bae, I. H.; Choi, J. K.; Chough, C.; Keum, S. J.; Kim, H.; Jang, S. K.; Kim, B. M. *ACS Med. Chem. Lett.* **2014,** *5* (3), 255-258.

23. Bouwstra, J. A.; Gooris, G. S.; Dubbelaar, F. E. R.; Ponec, M. *J. Invest. Dermatol.* **2002,** *118* (4), 606-617.

24. Fernandez, P.; Andre, V.; Rieger, J.; Kuhnle, A. *Colloid Surface A* **2004,** *251* (1-3), 53-58.

25. (a) Guillaume, O.; Garric, X.; Lavigne, J. P.; Van Den Berghe, H.; Coudane, J. *J. Control. Release* **2012,** *162* (3), 492-501; (b) Hwang, J. J.; Iyer, S. N.; Li, L. S.; Claussen, R.; Harrington, D. A.; Stupp, S. I. *P Natl. Acad. Sci.*

USA **2002,** *99* (15), 9662-9667.

26. Montenegro, L.; Campisi, A.; Sarpietro, M. G.; Carbone, C.; Acquaviva, R.; Raciti, G.; Puglisi, G. *Drug Dev. Ind. Pharm.* **2011,** *37* (6), 737-746.

27. Westesen, K.; Bunjes, H. *Int. J. Pharmaceut.* **1995,** *115* (1), 129-131.

28. Tadros, T. F. *Emulsion Formation, Stability, and Rheology. Emulsion Formation and Stability*; Wiley-VCH: Weinheim, Germany, 2013; pp 1-75.

29. Hirayama, F.; Uekama, K. *Adv. Drug Deliver. Rev.* **1999,** *36* (1), 125-141.

30. Muller, R. H.; Radtke, M.; Wissing, S. A. *Int. J. Pharmaceut.* **2002,** *242* (1-2), 121-128.

31. Amoozgar, Z.; Yeo, Y. *Wires Nanomed. Nanobi.* **2012,** *4* (2), 219-233.

32. Tamilvanan, S. *Prog. Lipid Res.* **2004,** *43* (6), 489-533.

33. Hua, S. *Int. J. Nanomed.* **2014,** *9*, 735-744.

국문초록

I. 편광측정법과 라만분광법을 이용한 액정에멀전의 구조 분석 및 레티닐 팔미테이트의 피부전달 영향 연구

분자량이 500이상으로 경피흡수에 어려움이 있는 레티닐팔미테이트의 경피전달체로 액정에멀전 연구를 진행하고 있다. 기존 보고된 경피약물전달체와는 달리 약물의 누출 가능성은 없으나, 제형의 경화 문제가 있어, 경화가 일어나지 않도록 계면활성제와 지방알콜, 에스테르류와 첨가물질의 조성비를 최적화하는 연구를 진행하였다. 계면활성제로 C12-20 알킬글루코시드, 솔비탄팔미테이트, 스테아릭애씨드, 글리세릴스테아레이트를 사용하고, 지방산으로 세틸알콜과 스테아릴알콜의 비율을 3:1로 하고, 에스테르는 카프릴릭/카프릭 트리글리세라이드를 사용하였을 때 육방정계 다중 층상 액정구조를 형성하는 것을 확인하였다. 경화 가속화 조건인 45도에서 3개월간 경화가 일어나지 않는 것을 확인하였고, 뮐러행렬편광계를 이용한 위상차를 비교하여 액정 구조의 안정성을 확인하였다. 라만공초점분광기으로 레티닐팔미테이트의 경피흡수 촉진을 평가하였을 때, 일반 에멀전 대비 95% 신뢰수준에서 최대 106%까지 촉진되는 것이 확인되었다. 본 연구에서 액정 에멀전의 경피 흡수 촉진은 뮐러행렬평광계를 이용한 위상차 평가에서 확인된 에멀전의 액정상과 피부의 액정상의 구조적 유사성에서 기인하는 것으로 유추할 수 있다.

II. 간에 선택적인 경구투여 약물전달 체계로서 액정나노입자 제형 연구

액정 나노입자는 약물의 생체 활성, 안정성 향상 및 표적약물 전달에 적합한 약물 전달 체계로서 연구되어 왔다. 이러한 액정 나노입자는 준비 과정에서 많은 에너지와 비용이 소요되는 것이 한계점으로 알려져 있어, 이러한 한계점을 극복하기 위해 지질, 계면활성제, 물의 조성비를 최적화하여 가열 및 냉각만으로 액정 나노입자가 제조 가능한 전상유화법을 연구하였다. 이러한 액정 나노입자는 약 100nm 크기로 사방정계 다중 층상 액정 구조로 구성되어 있는 것을 전자주사 현미경 및 X-선 회절분석을 통하여 확인하였다. 시험약물로 사용된 BMK-20113의 생체 활성이 향상되고, 지효성 약물 전달이 이루어지는 것을 약동학 시험에서 확인하였는데, 이러한 생체 활성 향상 및 지효성 약물 전달은 액정 나노입자의 다중 층상 구조에 의한 것으로 추론할 수 있다. 약물의 조직 분포 시험에서 간에서의 시험 약물 농도가 혈장에서의 농도보다 5.76배 높은 것을 확인하였다. 이러한 선택적 약물 전달은 본 연구의 액정 나노입자의 구조가 킬로마이크론과 유사하므로, 킬로마이크론의 대사과정에서 간에 흡수되는 것과 유사하게 액정 나노입자도 간에 선택적으로 흡수되는 것으로 추론할 수 있다.